Contributions to Characterization and Stochastic Modeling in the Presence of Nonlinear Active and Passive Circuits

Bijdragen tot karakterisering en stochastische modellering in aanwezigheid van niet-lineaire actieve en passieve circuits

Alessandro Biondi

Promotoren: prof. dr. ir. D. Vande Ginste, prof. dr. ir. D. De Zutter
Proefschrift ingediend tot het behalen van de graad van
Doctor in de Ingenieurswetenschappen: Elektrotechniek

Vakgroep Informatietechnologie
Voorzitter: prof. dr. ir. D. De Zutter
Faculteit Ingenieurswetenschappen en Architectuur
Academiejaar 2013 - 2014

UNIVERSITEIT GENT

ISBN 978-90-8578-656-6
NUR 959, 926
Wettelijk depot: D/2014/10.500/2

Acknowledgments

My first thanks goes to Prof. Daniël De Zutter for accepting me as a student of the Electromagnetics Group and giving me a chance to work towards my PhD degree. I would especially like to thank to my promoter, Prof. Dries Vande Ginste, for his patient guidance in the four year I spent as part of the EM-group. I would also like to thank Dr. Paolo Manfredi for our collaboration. Also, I would to like to spend some words for my friends for each moment we shared throughout this long period. My deepest gratitude goes to Joachim, for being so supportive and brilliant in every way. Also, I would like to thank my italian friends Damiano, L'Illustrissimo Dottore Luigi Vallozzi, La Mari, etc. Also, I would like to thank Marco, who has recently become part of the EM-group, from whom I have had the chance to learn a lot of things. My gratitude also goes to Arnaut and Sam for being so smart and funny. It was a great pleasure for me to spend time with you guys. Also, I would express my joy with my colleagues with whom I spent most of the times in the last four years. Last but not least, I would like to thank to my parents and my sister for their constant support. It is only thanks to them everything I achieved. To them I dedicate this thesis.

Alessandro Biondi
Gent, 9 January 2014

Logic will get you from A to B. Imagination will take you everywhere

ALBERT EINSTEIN

Contents

Samenvatting

Gestandaardiseerde elektromagnetische compatibiliteitsmetingen, kortweg EMC - metingen, beschouwen meestal een enkelvoudige bron die het te testen object (*device under test* – DUT) bestraalt met een monochromatisch signaal. Er zijn geen gangbare EMC-testen die scenario's met meervoudige bronnen en invallende signalen die meerdere frequentiecomponenten bevatten, in ogenschouw nemen. Daarom wordt na de algemene inleiding (Hoofdstuk 1) een nieuwe experimentele methode voorgesteld in Hoofdstuk 2, die bovenstaande lacune invult. De methode heeft als doel intermodulatiedistortie (IMD) te karakteriseren, een fenomeen dat typisch optreedt in sterk vervuilde elektromagnetische (EM) omgevingen die meerdere stoorbronnen bevatten. De nieuwe aanpak werkt voor algemene DUT's die op zijn minst één actieve component en één passieve, susceptibele antenne bevatten en dit dankzij de definitie van een aantal pertinente meetscenario's. We maken gebruik van een vectornetwerkanalysetoestel dat geschikt is voor niet-lineaire analyse, zoals de PNA-X van Agilent Technologies, en voeren de metingen uit in een gecontroleerde omgeving, bij voorkeur een anechoïsche kamer. Zo slagen we er in intermodulatie-(IM-)producten, desensitisatie, enz., opgewekt door de combinatie van gewenste in-de-band signalen en ongewenste buiten-de-band signalen, nauwkeurig te kwantificeren. Als testobject bestuderen we hiertoe een actieve textielantenne, geschikt voor de 2.45 GHz industriële, wetenschappelijke en medische (*Industrial, Scientific and Medical* – ISM) frequentieband.
Eerst analyseren en meten we het testobject in een klassieke meetopstelling via traditionele technieken. Dit laat toe de invloed van de afwezigheid van het ingangsfilter na te gaan. Dit filter, dat normaliter geplaatst is tussen het passief onderdeel, i.e. de antenne, en de actieve component, i.e. de lageruisversterker (*low noise amplifier* – LNA), is niet aanwezig om het systeem compact en goedkoop te houden. De afwezigheid kan echter leiden tot het lekken van frequentiecomponenten die zich buiten de band bevinden naar de gewenste ISM-band, en dit moet dus terdege worden onderzocht. Daarom worden daarna drie scenario's bekeken. In het eerste scenario wordt de DUT belicht met een monochromatisch signaal en valt een hogere-orde harmonische van dit signaal binnen de gewenste band. De harmonische is ongewenst en kan niet weggefilterd worden. Dit testscenario is dan ook belangrijk om te kunnen bestuderen in welke mate het stoorsignaal klein genoeg is ten opzichte van gewenste signalen en of het met andere woorden het EMC-gedrag van de DUT beïnvloedt. In het tweede scenario worden twee signalen beschouwd, waarbij het ene buiten de gewenste frequentieband ligt en het andere erbinnen. Deze signalen belichten het testobject en worden uitgestuurd

door twee bronnen die zich op dezelfde plaats bevinden. De twee frequentiecomponenten zorgen voor een IM-product dat binnen de gewenste band valt. In het derde scenario wordt de DUT belicht door een bron met een hoog zendvermogen en met een frequentie die buiten de band valt. Door het hoge vermogen functioneert de LNA van de actieve textielantenne niet meer naar behoren. De LNA heeft last van desensitisatie, waardoor zijn vermogensversterking en lineariteit afnemen, en dit resulteert in een te zwakke versterking van het gewenste signaal dat nu nog moeilijk te detecteren valt.
De invloed van de ongewenste harmonische, die plots opduikt in de gewenste band, kwantificeren we aan de hand van het stoorvrije dynamische bereik (*spurious free dynamic range* – SFDR). De invloed van zenders met een hoog zendvermogen, die desensitisatie van het circuit kunnen veroorzaken, wordt nagegaan aan de hand van de IM-producten die terug te vinden zijn aan de uitgang van de DUT en we bekijken ook de toon-vermogen-variatie (*Tone Power Variation* – TPV), i.e. de verhouding tussen het vermogen van het signaal dat wordt uitgestuurd door de stoorbron en het effectieve isotrope uitgestuurde vermogen (*effective isotropic radiated power* – EIRP) van de antenne die de DUT belicht. De testen tonen aan dat het mogelijk is actieve schakelingen met niet-lineaire componenten op kwantitatieve wijze te onderzoeken en na te gaan wat de invloed is van meerdere (stoor)bronnen die gewenste (binnen-de-band) en ongewenste (buiten-de-band) signalen uitsturen.

Naast EM-bewuste karakterisering, zoals hierboven beschreven, is ook de modellering van niet-lineaire circuits die werkzaam zijn op hoge frequenties van het grootste belang. Binnen deze context stellen we een aantal nieuwe stochastische simulatietechnieken voor. Meer bepaald bestuderen we hogesnelheidsinterconnectiestructuren omdat hun productieproces onzekerheid introduceert qua geometrische dimensies en materiaaleigenschappen van deze structuren. Variabiliteit, veroorzaakt door het productieproces, leidt tot niet-deterministisch gedrag en noopt ons ertoe stochastische modelleringsmethodes te ontwikkelen. De typische methode om statistische informatie te verzamelen van systemen die onderhevig zijn aan variabiliteit, is de Monte Carlo (MC) methode. Deze methode is waarschijnlijk de meest gekende en meest gebruikte omdat ze robuust is en eenvoudig te implementeren. Nochtans is er een groot nadeel verbonden aan de MC techniek. Het is namelijk zo dat een groot aantal monsters vereist is om nauwkeurige resultaten te bekomen. De MC techniek kan dan ook niet gebruikt worden wanneer de rekentijd die nodig is om één enkel monster te simuleren, groot is. Het doel van dit werk is om alternatieve en efficiëntere strategieën te bedenken.

De bovenstaande tekortkomingen van de MC methode worden overwonnen door techieken te ontwikkelen die gebaseerd zijn op de zogenaamde polynomiale chaos-(PC-)theorie. Meer bepaald beschouwen we in onderhavig werk een stochastische Galerkinmethode (SGM) voor multigeleiderlijnen die beschreven worden door de telegraafvergelijkingen. In de recente literatuur zijn reeds PC-gebaseerde technieken terug te vinden voor interconnectiestructuren die belast worden met lineaire compo-

nenten en voor circuits bestaande uit lineaire en zwak niet-lineaire discrete componenten. In deze doctoraatsthesis zullen we echter een SGM aanbieden die het mogelijk maakt stochastische multigeleiderlijnen te belasten met generieke niet-lineaire componenten, beschreven door algemene I-V-karakteristieken (Hoofdstuk 3) of door polynomiale I-V-karakteristieken (Hoofdstuk 4). Dit wordt mogelijk gemaakt door de SGM te combineren met de tijdsdomein-eindige-differentiemethode (*finite-difference time-domain* – FDTD). In Hoofdstuk 3 worden de algemene niet-lineaire belastingen beschreven door een benaderende relatie tussen de stroom- en spanningscoëfficiënten aan de klemmen van de component, die verder wordt behandeld met numerieke integratie via Gaussische kwadratuurschema's. De SGM-FDTD techniek is geïmplementeerd in Matlab en maakt gebruik van de $\mathrm{fsolve.m}$ routine om de wortels van de pertinente set gekoppelde niet-lineaire vergelijkingen te vinden. Voor wat betreft belastingen met polynomiale I-V-karakteristieken wordt in Hoofdstuk 4 een nog efficiëntere methode voorgesteld. Voor dit type belastingen kan immers gebruik gemaakt worden van exacte, analytische integratie. Beide technieken worden gevalideerd en geïllustreerd aan de hand van voorbeelden die bestaan uit (gekoppelde) miscrostriplijnen die onderhevig zijn aan variabiliteit. Meer bepaald vertonen zowel hun geometrische dimensies als hun materiaaleigenschappen onzekerheid. De lijnen worden afgesloten met een diode met een niet-gladde I-V-karakteristiek of met een niet-lineaire condensator met een polynomiale I-V-karakteristiek. In beide gevallen nemen we een heel goede overeenkomst met de resultaten verkregen via een klassieke MC analyse waar. Bovendien hebben de nieuwe methodes een veel kortere rekentijd.

De technieken beschreven Hoodstukken 3 en 4 zijn geïmplementeerd in Matlab. Ze zijn daarenboven gebaseerd op FDTD, wat het moeilijk maakt om verlieshebbende, dispersieve interconnectiestructuren en willekeurige netwerktopologieën te bestuderen. Daarom worden ze in het vijfde hoofdstuk aangepast zodat ze kunnen geïntegreerd worden binnen een SPICE-omgeving. SPICE staat voor *Simulation Program with Integrated Circuit Emphasis*, een vaakgebruikte ontwerpsomgeving. Er wordt in Hoofdstuk 5 een SPICE-compatibele methode ontwikkeld en geïmplementeerd in deze traditionele omgeving en dit laat toe om PC-gebaseerde variabiliteitsanalyses van verlieshebbende, dispersieve transmissielijnen met algemene niet-lineaire belastingen door te voeren. Zodoende kan deze techniek nu ook gebruikt worden door ontwerpsingenieurs. Opnieuw wordt een zeer goede nauwkeurigheid ten opzichte van de MC methode waargenomen en de nieuwe techniek is veel sneller.

In deze doctoraatsthesis wordt aangetoond dat EM-bewuste karakterisering van niet-lineaire componenten, zoals beschreven in Hoofdstuk 2, toelaat om op accurate wijze nieuwe systemen te testen zodoende duur en tijdrovend herontwerp te vermijden. De stochastische simulatiemethodes, voorgesteld in Hoofdstukken 3, 4 en 5, leveren een belangrijke bijdrage tot het onderzoek naar (de analyse van) variabiliteit van elektronische systemen en dienen hetzelfde doel. Voor beide aspecten, karakterisering en modellering, wordt ruim aandacht besteed aan de aanwezigheid van niet-lineaire

componenten, dit in tegenstelling tot meer traditionele methodes. Zoals ook vermeld in Hoofdstuk 6, is de auteur er immers van overtuigd dat verder onderzoek in dit domein van het hoogste belang is voor de verdere ontwikkeling van nieuwe elektronische systemen.

Summary

Standard electromagnetic compatibility (EMC) testing procedures most often focus on single-source/single-frequency illumination of the devices under test (DUT). There are no conventional test practices that involve multi-source/multi-frequency testing. Therefore, after a general introduction in Chapter 1, we propose in Chapter 2 a new experimental technique to characterize intermodulation (IM) distortion phenomena that typically occur in noisy electromagnetic (EM) environments, which contain multiple (co-located) sources. This new approach is suitable for any generic DUT composed of at least one active nonlinear component and a passive susceptible antenna by clearly defining a set of pertinent measurement scenarios. By means of a vector network analyzer that allows nonlinear analysis, such as Agilent's PNA-X, and in a controllable environment, preferably an anechoic chamber, we show that IM products, desensitization, etc., induced by a combination of desired, in-the-band, and undesired, out-of-band, signals can be accurately quantified. In our case, an active textile antenna is used as test bench to prove the effectiveness of the new approach with the 2.45 GHz Industrial, Scientific and Medical Radio (ISM) band as the frequency band of interest. First, we analyze and measure the device in a stand-alone configuration. In particular, the influence of the absence of a filter in between the susceptible device and the nonlinear component is investigated as this might allow undesired out-of-band signals to leak into the frequency band of operation. Three different transmitting scenarios are considered. In the first scenario a transmitter illuminates the DUT with a single frequency component and a higher-order harmonic falls into the band of interest as unwanted signal. Once this occurs, the unwanted signal can no longer be removed by filtering. Therefore, it is important to test whether the power of this in-the-band disturbance remains small enough compared to the desired signal, in order not to affect the EMC performance of the DUT. In the second scenario two tones, a desired one falling in the band and an unwanted one falling out-of-band, radiated by co-located sources illuminate the DUT. The two frequency components result in an IM product falling in the band of operation. In the third scenario, a high power out-of-band transmitter is illuminating the DUT. Because of its high power, the low-noise amplifier (LNA) of the active textile antenna does no longer operate as expected. The LNA gets desensitized, i.e. gain and linearity decrease, resulting in a desired signal that is less amplified and hence more difficult to detect.

To characterize the effect of harmonics of the out-of-band frequency turning up in the frequency band of interest, the spurious free dynamic range (SFDR) is put forward

as a suitable measure. Furthermore, the influence of strong transmitters, that might desensitize the LNA, on the relative importance of IM products in the DUT's output spectrum is examined. As a measure for the desensitization, we introduce the Tone Power Variation (TPV) parameter, i.e. the ratio of the power of a particular tone to the Effective Isotropic Radiated Power (EIRP) of the antenna used to illuminate the DUT. The series of tests demonstrate that quantitative testing of active DUTs with nonlinear components illuminated by multiple co-located sources emitting both desired, in-the-band, and undesired, out-of-band, signals can be successfully carried out using an anechoic chamber, standard gain horns, a PNA-X network analyzer and a well-chosen linear preamplifier together with a set of clear measurement scenarios.

Next to EM-aware characterization, the modeling of nonlinear circuits subjected to high-frequency phenomena is also of critical importance. Within this context, we propose new stochastic simulation techniques. More specifically, we focus on high-speed interconnects, as their manufacturing process causes geometrical and material parameter uncertainties. This variability leads to nondeterministic behavior, and hence necessitates the development of proper stochastic modeling tools. The classical resource to gather statistical information is the Monte Carlo (MC) method. The MC method is perhaps the most common algorithm employed for the stochastic simulation of arbitrary systems affected by random variations, due to its robustness and its relative simplicity. Nevertheless, the main drawback of MC is that it requires a large number of samples to converge. Therefore, this approach becomes unfeasible when the time required by a single simulation is large. Hence, the goal of this work is to provide an alternative and more efficient strategy.

To overcome the aforementioned difficulties, we develop a stochastic analysis method for interconnect structures based on the so-called polynomial chaos (PC) theory, more specifically a stochastic Galerkin method (SGM) for multiconductor lines governed by the transmission line equations. In recent literature, PC-based techniques have been developed for distributed interconnects terminated by linear loads and for stochastic lumped circuits, but only taking mild nonlinearities into account. In contrast, the novel SGM framework advocated in this work is capable of also including general nonlinear loads, described by arbitrary I-V-characteristics (Chapter 3) and by polynomial I-V-characteristic (Chapter 4), at the terminals of stochastic multiconductor transmission lines (MTLs). This is made possible by combining the SGM with a standard finite-difference time-domain (FDTD) method for MTLs. To include arbitrary nonlinear loads, in Chapter 3 we construct an approximate analytical relationship between the current and voltage expansion coefficients at the terminals of the lines, adopting a numerical integration scheme based on Gaussian cubatures. The SGM-FDTD is implemented in Matlab and makes use of the $\mathrm{fsolve.m}$ routine, which allows to find the roots of a set of coupled nonlinear equations. For polynomial I-V-characteristics, a more efficient scheme is constructed (Chapter 4), via exact closed-form solutions of the pertinent integrals. Both proposed techniques were validated and

illustrated by means of application examples, consisting of (coupled) microstrip lines exhibiting variability of their geometrical and material parameters, and terminated by a diode with a non-smooth I-V-characteristic or by a nonlinear capacitor described by a polynomial model. In both cases, we observed an excellent agreement as compared to the standard MC method and a far superior efficiency in terms of runtime.

The above techniques, presented in Chapters 3 and 4, are implemented in Matlab. As this approach relies on a FDTD solver for transmission lines, dealing with lossy, dispersive lines and arbitrary circuit topologies is rather cumbersome. For this reason, the technique presented in Chapter 3 is adapted in Chapter 5. In fact, a SPICE-compatible method is developed and implemented in a traditional design environment allowing for the first time to perform PC-based variability analyses of lossy, dispersive MTLs terminated by general nonlinear loads. The goal is to make this technique more accessible for designers via integration in a commercial tool. Also in this case, excellent agreement between the MC reference results and the ones obtained by using the novel implementation is obtained, and the new method is much more efficient.

This dissertation clearly illustrates that EM-aware characterization of nonlinear devices, as proposed in Chapter 2, allows designers to more accurately test new devices without the need of many time-expensive and costly redesigns. The stochastic methods proposed in Chapters 3, 4 and 5 yield a considerable contribution to the research on stochastic simulation techniques and serve the same design purpose. For both aspects, characterization and modeling, and in contrast to many traditional approaches, the inclusion of nonlinear circuit elements is studied. As also stated in Chapter 6, after all, the author is convinced that further investigations in this domain are of critical importance for the development of state-of-the-art electronic devices.

List of Abbreviations

ADS	Advanced Design System
BC	Boundary Condition
CDF	Cumulative Distribution Function
DUT	Device Under Test
EIRP	Equivalent Isotropically Radiated Power
EM	Electromagnetism / Electromagnetic
EMC	Electromagnetic Compatibility
EMI	Electromagnetic Interference
FDTD	Finite-Difference Time-Domain
FET	Field-Effect Transistor
FEXT	Far-End Cross-Talk
gPC	Generalized Polynomial Chaos
I	Current
IEEE	Institute of Electrical and Electronics Engineers
IET	Institution of Engineering and Technology
IM	Intermodulation
IMD	Intermodulation Distortion
ISM	Industrial, Scientific and Medical Radio Bands
LNA	Low Noise Amplifier
MC	Monte Carlo
MTL	Multiconductor Transmission Line
NEXT	Near-End Cross-Talk
NF	Noise Floor
OIP2	Second-Order Intercept Point
OIP3	Third-Order Intercept Point
PA	Power Amplifier
PC	Polynomial Chaos
PDF	Probability Density Function
PL	Path Loss
RF	Radio Frequency
RV	Random Variable
SCM	Stochastic Collocation Method
SDR	Software Defined Radio
SFDR	Spurious Free Dynamic Range

SGM	Stochastic Galerkin Method
TA	Transmission Attenuation
TPV	Tone Power Variation
V	Voltage

List of Publications

Articles in international journals

- A. Biondi, L. Vallozzi, F. Declercq, D. De Zutter, H. Rogier, "EMC aware design and testing of intermodulation distortion under multiple co-located sources illumination", *IET Science, Measurement & Technology*, Vol. 6, no. 2, pp. 105 – 112, Mar. 2012

- A. Biondi, D. Vande Ginste, D. De Zutter, P. Manfredi, F. Canavero, "Variability Analysis of Interconnects Terminated by General Nonlinear Loads ", *IEEE Transactions on Components, Packaging, and Manufacturing Technology* , Vol. 3, no. 7, pp. 1244 – 1251, May. 2013

Submitted manuscripts to international journals

- A. Biondi, D. Vande Ginste, D. De Zutter, P. Manfredi, F. Canavero, "Variability Analysis of Interconnect Structures Including General Nonlinear Elements in a SPICE-type Framework ", *IET Electronic Letters*

Articles in conference proceedings

- A. Biondi, D. Vande Ginste, D. De Zutter, H. Rogier, "Multi-tone EMC testing strategy for RF-devices ", *Electrical Design of Advanced Packaging & Systems (EDAPS)*, Taipei, Taiwan, 9 – 11 Dec 2012, pp. 89 – 92
  Winner of the Best Poster Paper Award

Accepted manuscripts for conference proceedings

- A. Biondi, D. Vande Ginste, D. De Zutter, P. Manfredi, F. Canavero, "Variability Analysis of Interconnects Terminated by Polynomial Nonlinear Loads", Accepted for *Electrical Design of Advanced Packaging & Systems (EDAPS)*, Nara, Japan, 11 – 15 Dec. 2013

Contributions to Characterization and Stochastic Modeling in the Presence of Nonlinear Active and Passive Circuits

CHAPTER 1
Introduction

In the last centuries an impressive development in electronic technology was brought to life. In the 19^{th} century, James Clerk Maxwell's publications in 1864 about the theory that unified electrodynamics, magnetodynamics and optics revealed the existence of the electromagnetic (EM) waves. Not without initial skepticism, his theory was experimentally tested by Heinrich Rudolf Hertz in 1865, who used spark discharges to produce EM waves, as such indeed proving their existence. In 1894, a very talented Italian inventor, Guglielmo Marconi, at age twenty-two, patented a successful system of radio telegraphy, which would revolutionize the world of communication, awarding him the Nobel Prize. In 1901, Marconi even succeeded in transmitting signals across the Atlantic Ocean. Soon after, Marconi's Wireless Telegraphy Company established a net of coast stations in Britain for ship-to-shore communication, defining a standard for wireless communication for more than two decades [1].

On the other hand in the 20^{th} century, the invention of the transistor propelled electronics ages forward. In 1907, the first vacuum tube was invented, known as thermionic triode. It allowed amplifying radio signals and hence it eased long distance communication. Unfortunately, the thermionic triode was fragile and not power-efficient. In 1925, Julius Edgar Lilienfield patented the Field-Effect Transistor (FET), which was intended to be a solid-state replacement for the thermionic triode. Later, in the 1940s, John Bardeen, Walter Brattain and William Shockley, resident scientists at AT&T's Bell Labs in the United States, performed experiments and observed that by applying two gold point contacts to a crystal of germanium, a signal was produced with an output power higher than the input [2]. Nevertheless, only after many years of research and development, the first commercial high-frequency transistor was brought to life, being the surface-barrier germanium transistor, developed by Philco in 1953 and capable of operating up to 60 MHz [3]. Soon after, the transistor became a key active component for the development of more complex electronic structures. Its importance in today's society stems from its ability to be mass-produced in so-called integrated circuits by means of a highly automated manufacturing process. The transistor's low cost, high flexibility and overall reliability have made it a ubiquitous

device.

This technological boost came at a cost. During the last decades, we witnessed the ever advancing increase in clock and bit rates, as well as an increase in complexity of electronic systems. State-of-the-art devices have multiple functionalities and they are highly miniaturized. All this led to ever more stringent design specifications, expressed in terms of speed, bandwidth, crosstalk, etc, rendering electronic design increasingly more complex. On top of that, national and international regulations require rigorous electromagnetic compatibility (EMC) compliance [4], complicating the matter even further.

To cope with this increasing level of complexity, on the one hand, designers rely on simulation and design software. In the early design phase of a product, accurate predictions by means of these tools may lead to right-the-first-time designs, minimizing the need for expensive measurement campaigns and overall refabrication. So far, however, most simulation tools are constructed to perform *deterministic* simulations, meaning that the modeled device is exactly known. Nowadays, this is no longer the case. Many parameters of the design, such as material or geometrical parameters, are prone to, e.g., manufacturing tolerances, fluctuations in operating temperature, uncontrollable parameters, aging, etc. In particular for miniaturized systems, these tolerances may lead to system malfunction, because the nominal design, as deviced and desired by the electronic engineer, may differ substantially from the manufactured end product. Therefore, there is a high need for efficient simulation tools that can deal with this kind of variability and randomness of design parameters.

On the other hand, designers often have to resort to experimental methodologies to evaluate the performance of their devices. Many simulation tools are simply not yet powerful enough to model very complex problems, such as e.g. assessing the immunity behavior of high-frequency devices in a very polluted EM environment [5]. Nonetheless, the copious amount of electronic devices in our every day life necessitates the ability to operate under these conditions.

The goal of this doctoral research is to construct novel simulation and measurement techniques that can deal with the above described issues. In contrast to previous successful research, such as [6], special attention is devoted to the assessment of the EM behavior of *nonlinear* circuits and devices.

1.1 EM-aware characterization and modeling of nonlinear circuits

A nonlinear device comprises at least one circuit element for which a linear relationship between the currents (I) and the voltages (V) at the element's port does not exist. A typical example of a nonlinear element is a diode. Other examples include transistors, vacuum tubes, iron core inductors and transformers when operated above their

saturation currents, mixers, amplifiers, transceivers, etc. In reality, most electrical elements are nonlinear, but for some of them, e.g. resistor, capacitors, inductors, the I-V-response can be approximated by means of a linear characteristic.

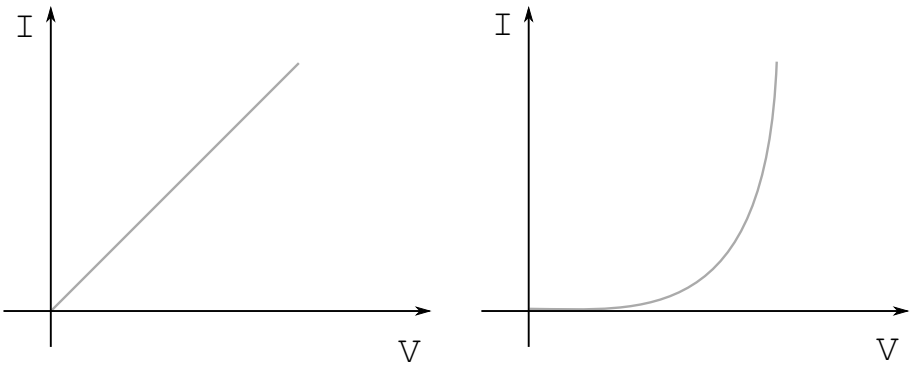

Figure 1.1: Linear I-V characteristic (left), nonlinear I-V characteristic (right)

Nonlinear elements play a crucial role in state-of-the-art electronic design. In fact, the majority of the devices, such as computers, smartphones etc., would not function without the presence of nonlinear elements, thus it is important to evaluate their influence. A simplified graphical representation of linear vs. nonlinear behavior is sketched in Fig. 1.1.

During the last years, growing interest has emerged in the development of compact, low-cost, low-power, reconfigurable microwave systems. To allow miniaturization and to reduce costs, radio frequency (RF) filters in front of active devices [7] should be omitted. Also, in software defined radio (SDR), the use of RF filters is prohibited, as a very broadband signal is received by the antenna and directly amplified, before being converted to the digital domain, where further processing takes place [8]. Nonlinearities in such devices combined with the lack of filtering may compromise performance. Signal integrity (SI) and EMC [9, 10] are affected due to in-the-band leakage of out-of-band undesired signals interfering with the desired signal. Indeed, when two or more signals are present at the input of a nonlinear component, in addition to the wanted signal, the signal at the output of that component includes other frequency components due to intermodulation (IM) distortion. This issue in particular arises when several sources illuminate a RF device, although maybe none of these sources would compromise SI or EMC by themselves [5]. Hence, these phenomena become more and more important when multiple users are sharing the same electromagnetic environment, as schematically shown in Fig. 1.2. Given the high diffusion of RF devices in our every day life, their ability to operate properly in their electromagnetic environment, i.e. to function without being influenced or without causing electromagnetic interference (EMI) is of critical importance [11] .

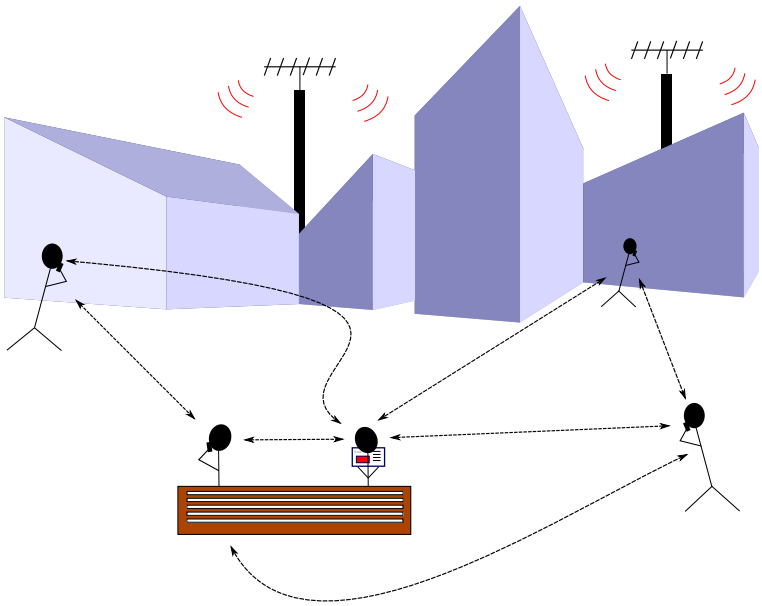

Figure 1.2: Sketch of a typical transmissive scenario in the presence of different users.

1.2 State-of-the-art and problem statement

Current electromagnetic immunity tests mainly rely on single-frequency sources [9]. However, as stated above, it is crucial to evaluate the performance when other RF devices are in the vicinity. Within this context, the following observations are made:

- EMC testing, and compliance tests in general, rely on standardization, and mostly aim at accuracy and repeatability rather than mimicking a typical exposure set-up.
- Classical standardization immunity tests do not consider the simultaneous illumination of the system under test by multiple RF sources.
- The application of more than one disturbance potentially results in severe compromise of EMI immunity, due to the presence of nonlinearities.

Therefore, in this dissertation, novel EMC testing strategies are conceived and implemented to account for the above described effects.

Within the numerical simulation context there are some considerations that need to be made. The stochastic simulation environment can be further enriched with regards to traditional approaches used to gather statistical information. In fact, the traditional way to gather statistical information relies on the well-known Monte Carlo (MC)

method. A new approach to the stochastic analyses of arbitrary interconnecting structures can be found in the so-called Polynomial Chaos (PC) method, which has been successfully used to approach the analysis of single or multiconductor lines governed by the so-called transmission-line equations. State-of-the-art PC-based methods are, however, only developed for circuits composed of lumped elements that are linear or mildly nonlinear [12, 13] and for distributed elements (i.e. transmission lines) that are terminated by linear loads [14], [15]. In this work, we aim to conceive efficient and accurate stochastic modeling techniques for interconnect structures in the presence of general nonlinear loads.

1.3 Organization of the text

The remainder of this doctoral thesis is organized as follows. In Chapter 2, a comprehensive strategy consisting of design and test methodologies to evaluate in-the-band leakage of out-of-band undesired components, using multi-tone excitation and relying on an anechoic chamber as test facility, is presented. The aim of this chapter is to demonstrate that an anechoic chamber together with a dual-source network analyzer represents an optimal facility to investigate signal integrity issues due to leakage of intermodulation products. In Chapter 3, a dedicated stochastic modeling method, implemented in Matlab, is presented for the analysis of variability effects, induced by the manufacturing process, on interconnect structures terminated by general nonlinear loads. The technique is based on the solution of the pertinent stochastic Telegrapher's equations in time domain by means of the well-established stochastic Galerkin method, allowing the inclusion of loads with arbitrary I-V-characteristics at the terminals of the lines. The technique is optimized in Chapter 4 to even more efficiently deal with loads for which there exists a polynomial relationship between the current and the voltage. In Chapter 5, it is shown that this technique can also be implemented in a commercial framework such as HSPICE, rather than Matlab. This brings about many advantages for the design engineer. In the last chapter, the main conclusions are presented and an outline for future research is suggested.

Bibliography

[1] P. K. Bondyopadhyay, "Guglielmo Marconi, the father of long distance radio communication," in *Proceedings of the 25th European Microwave Conference*, Bologna, Italy, 1995, p. 879.

[2] B. L. AT&T, "History of Bell Labs." [Online]. Available: http://www.corp.att.com

[3] R. Bray, *The Origin of Semiconductor Research at Purdue*. Purdue University, Department of Physics, 1989.

[4] C. R. Paul, *Analysis of Multiconductor Transmission Lines*. John Wiley & Sons, 1994.

[5] Duffy, A., Orlandi, A. , Armstrong, K., "Preliminary study of a reverberation chamber method for multiple-source testing using intermodulation," *IET Sci. Meas. Technol.*, vol. 4, pp. 21–27, 2010.

[6] C. Gadza, "Electromagnetic compatibility and signal integrity aware modeling and design of electronic circuits," Doctoral thesis, Dept. of Information Technology – Ghent University, Ghent, Belgium, 2012.

[7] A. Rembovsky, A. Ashikhmin, V. Kozmin, S. Smolskiy, *Radio Monitoring: Problems, Methods and Equipment*, 1st ed. Springer, 2009.

[8] P. Cruz and K. Remley, "Designing and testing software designed radios," *IEEE Microwave Magazine*, pp. 83–94, Jun. 2010.

[9] M. Mardiguian, "Combined effects of several simultaneous, EMI couplings," vol. 1, Washington, August 2000, pp. 181–184.

[10] E. S. J. Nitsch, N. Korovkin and H.-J. Scheibe, "Occurrence of low-frequency noises in electronic systems under action of two-tone high frequency electromagnetic excitation," vol. 2, Magdeburg, Aug. 2005, pp. 618–621.

[11] M. I. Montrose, *EMC and the Printed Circuit Board: Design, Theory, and Layout Made Simple*. IEEE Press, Piscataway, NJ, USA, 1999.

[12] Q. Su and K. Strunz, "Stochastic circuit modelling with Hermite polynomial chaos," *Electronic Letters*, vol. 41, no. 21, pp. 1163–1165, Oct. 2005.

[13] K. Strunz and Q. Su, "Stochastic formulation of SPICE-type electronic circuit simulation with polynomial chaos," *ACM Trans. on Modeling and Computer Simulation*, vol. 18, no. 4, pp. 15:1–15:23, Sep. 2008.

[14] P. Manfredi, D. Vande Ginste, D. De Zutter, and F. G. Canavero, "Uncertainty assessment of lossy and dispersive lines in SPICE-type environments," *IEEE Transactions on Components, Packaging and Manufacturing Technology*, vol. 3, no. 7, pp. 1252–1258, Jul. 2013.

[15] P. Manfredi, D. Vande Ginste, D. De Zutter, and F. G. Canavero, "On the passivity of polynomial chaos-based augmented models for stochastic circuits," *IEEE Trans. on Circuits and Systems*, vol. PP, pp. 1–10, Jul. 2013.

CHAPTER 2

EMC aware characterization of intermodulation distortion under multiple co-located sources illumination

Based on the publications:

"EMC aware design and testing of intermodulation distortion under multiple co-located sources illumination", *IET, Science, Measurements & Technology*, Vol. 6, no. 2, pp. 105-112, Mar. 2012

"Multi-Tone EMC Testing Strategy for RF-Devices",
Electrical Design of Advanced Packaging and Systems Symposium (EDAPS), 2012, IEEE Taipei, Taiwan, 9 – 11 Dec 2012, pp. 89-92
Winner of the Best Poster Paper Award

Current electromagnetic immunity tests mainly rely on single-frequency sources. However, the evolution of electronic systems leads to miniaturization and low-cost solutions, in which filters are omitted in front of active nonlinear components, also for efficiency reasons. As a result, intermodulation products may leak into the band of operation. We propose a comprehensive strategy consisting of design and test methodologies to evaluate in-the-band leakage of out-of-band undesired components, using multiple-tone excitation and relying on an anechoic chamber as test facility. The aim of this chapter is to demonstrate that an anechoic chamber together with a dual-source network analyzer represents an optimal facility to investigate signal integrity issues due to leakage of intermodulation products.

2.1 Introduction

In the last years, a great interest has emerged in the development of compact, low-cost, low-power, reconfigurable microwave systems. This evolution led to miniaturized, low-cost solutions, in which filters in front of active devices [1] may be omitted. For instance, in software defined radio (SDR), a very broadband signal is received by the antenna and directly amplified, before being converted to the digital domain, where further processing, including filtering, takes place [2]. nonlinearities in these devices combined with the lack of shielding and filtering may compromise performance, signal integrity and electromagnetic (EM) compatibility [3–5] due to in-the-band leakage of out-of-band undesired signals interfering with the desired signal. Indeed, when two or more signals are present at the input of a nonlinear component, the signal at the output of that component includes other frequency components in addition to the wanted signals due to intermodulation (IM) distortion. This issue in particular arises when several sources illuminate devices under test (DUTs), where none of the sources will individually compromise signal integrity (SI) or EM immunity (EMI) but the total effect of these sources is such as to potentially cause SI and EM compatibility (EMC) problems [6].

Therefore, in contrast to existing established EMC tests, it is important to develop and understand approaches to test electronic systems under multiple-sources illumination, in particular when IM products occur that might potentially disturb the DUT and cause SI/EMI issues. Existing EMC tests rely on single frequency sources, and thereby do not always provide a realistic transmission scenario [6], [7].

Hence, in this chapter, we present a comprehensive experimental strategy to model and test RF devices under multiple frequency sources illumination, in the presence of out-of-band frequency components leaking into the band of interest. Specifically, the novel contributions are: (i) a new EMC aware computer-aided design strategy is outlined providing guidelines to account for in-the-band leakage of undesired out-of-band signals due to IM distortion. It is demonstrated how the current use of standard

parameters describing nonlinearities, such as $P_{1\text{dB}}$, OIP_2 and OIP_3 often fail to capture leakage effects; (ii) novel precompliance tests using a dual-source Vector Network Analyzer are proposed at the subsystem/device level to quickly identify and correct for IM distortion during the design; (iii) new EMC tests are defined to characterize in-the-band leakage of a DUT, using an anechoic chamber and multiple co-located interfering sources transmitted along the main beam of the illuminating antenna, as such representing the worst-case transmission scenario. Test procedures are outlined where the DUT is tested at different radiated power levels and at varying distances.

The organization of the chapter is as follows. First, the different mechanisms that lead to in-the band leakage of undesired signals via IM distortion are discussed in the next section. This allows us to define modelling and test procedures during the design, precompliance as well as compliance testing phases. Sections 2.3 and 2.4 discuss the practical implementation of this strategy for a representative circuit, consisting of an antenna that picks up the disturbing signals in a frequency-selective way combined with a low-noise amplifier (LNA) that creates intermodulation distortion (IMD) due to its nonlinearity. Specifically, in the design and precompliance testing phase, as discussed in Section 2.3, the focus is on the nonlinear device, tested and modeled in a 50Ω environment. Section 2.4 focusses on testing the complete DUT for EMC compliance. Section 2.5 summarizes the conclusions of the chapter.

2.2 Accounting for IM Distortion in EMC Aware Design and Testing

In this section we put forward a strategy to evaluate the behavior of a DUT (Fig. 2.1) under multiple-sources' illumination. In particular, we must account for all different causes of IM products that might give rise to in-the-band leakage.

2.2.1 Causes of IM distortion

Electronic devices are susceptible to different kinds of disturbances depending on their nature. In order for a component device or system to be susceptible to multi-frequency signals it must consist of a concatenation of a susceptible linear device, and a nonlinear component creating IM products. Specifically, it is the absence of a filter in between the susceptible device and the nonlinear component in Fig. 2.1 that allows undesired out-of-band signals to leak into the frequency band of operation. To provide a clear view to the EMC aware design and test engineer, we first present the different scenarios resulting in IM distortion. Each cause of IM products, leading to potential in-the-band leakage of unwanted signals due to IM distortion, corresponds to a specific multi-frequency transmission scenario that will be recreated in the design, precompliance and compliance testing phase by means of modeling and experiments. Fig. 2.2

shows the case in which a transmitter illuminates the DUT with a single frequency component (tone) at f_0, and a higher-order (the second-order in the figure) harmonic falls into the band of interest as unwanted signal (*scenario 1*). Once this occurs, the unwanted signal can no longer be removed by filtering. Therefore, it is important to test whether the power of this in-the-band disturbance remains small enough compared to the desired signal, in order not to affect the EMC performance of the DUT.

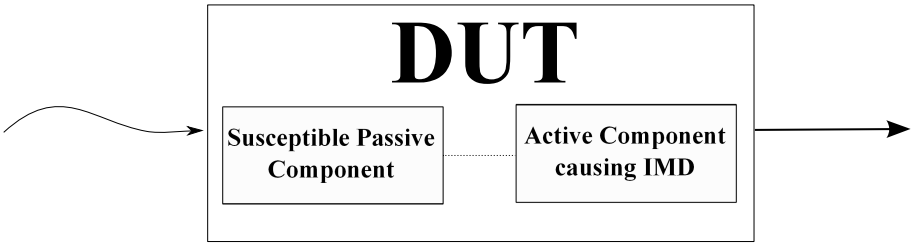

Figure 2.1: A general DUT.

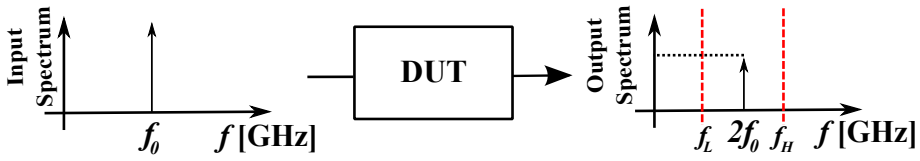

Figure 2.2: Propagation of harmonics in the output spectrum of the DUT (scenario 1).

The *second scenario*, represented in Fig. 2.3, depicts the case of two tones, f_1 and f_2, a desired one f_1 falling in the band, and an unwanted one f_2 falling out-of-band, radiated by the co-located sources illuminating the DUT (two possible cases $f_2 < f_1$ or $f_2 > f_1$). In this scenario the two frequency components result in an intermodulation product falling in the band of operation of the device. Again, the power of the in-the-band interference should be monitored to validate the EMC behavior of the DUT. The results reported later in Section 2.4 only consider the case $f_2 < f_1$ but similar results could be obtained for $f_2 > f_1$. Note that also two undesired out-of-band signals generating relevant in-the-band interference should be considered in this scenario, although such a configuration is not illustrated in the sequel for reasons of conciseness.

Finally, Fig. 4 depicts a *third scenario* in which a high power out-of-band transmitter (frequency f_2) is illuminating the DUT. Because of its high power, the LNA does no longer operate as expected. The LNA gets desensitized i.e. gain and linearity decrease, resulting in a desired signal that is less amplified and hence more difficult to detect. Also this scenario should be accounted for in EMC aware design and suitable

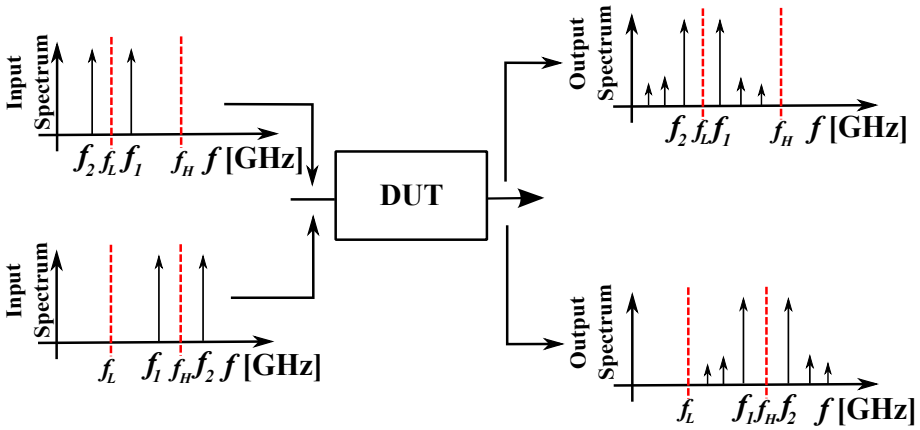

Figure 2.3: Response of the DUT to an in-the-band tone f_1 and an out-of-band tone f_2 (scenario 2).

tests must be established to ensure EM compatibility of the DUT.

At this point we should make two important remarks: First, from Fig. 2.4 it is seen that the undesired signal that desensitizes the amplifier may also result in important in-the-band IM products, as studied in scenario two. In such a case, the desensitization will further decrease the ratio of the power of the desired signal over the power of the IM distortion, as the wanted signal gets less amplified whereas the unwanted signal increases more than expected with rising signals levels. Second, a strong out-of-band signal may desensitize the DUT without producing IM products in the desired frequency band. This process may, however, make the DUT more sensitive to IM products produced by other out-of-band signals. This, rather complex, scenario is not further investigated for reasons of conciseness.

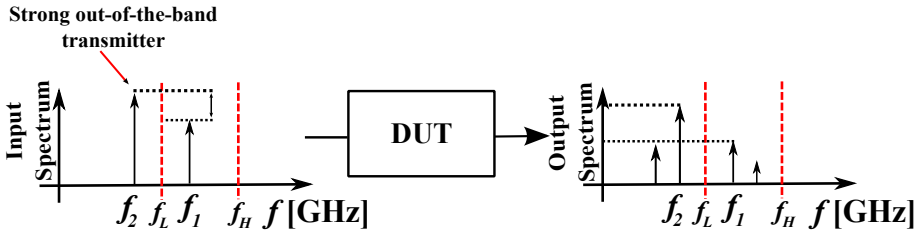

Figure 2.4: Desensitization due to an out-of-band tone f_2 (scenario 3).

2.2.2 Design and precompliance/compliance testing strategies

To be able to include IM distortion during the *EMC aware design phase*, the interfering multi-frequency signals will be applied as sources in a full-wave/circuit co-simulation, whereas during *precompliance tests* these simulated results are verified at the subsystem and module levels by performing direct multi-tone injection by means of an Agilent N5242A PNA-X network analyzer. Testing all subsystems/modules separately provides a quick way for early diagnostics during design and precompliance testing, but it does not provide a complete picture, since input and/or output of the subsystem/module under test act as frequency-dependent loads over the broad frequency range over which unwanted signals will impinge, and this is not taken into account when using a network analyzer, which tests the subsystem/module in a constant 50 Ω environment.

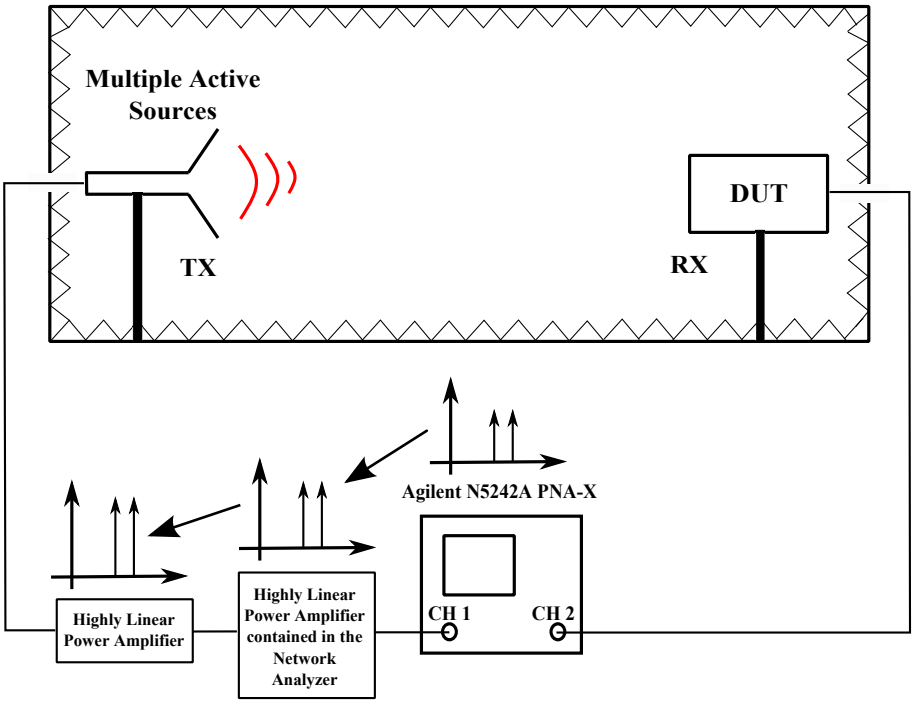

Figure 2.5: Anechoic Chamber Setup.

Therefore in the final *compliance tests* the multi-frequency signals are transmitted by a standard gain horn letting them impinge in the far-field on the complete DUT. In Fig. 2.5 we propose the setup for such a multi-frequency test to be performed in an anechoic chamber. The transmission source in the experiment is a standard gain horn, connected to a highly-linear power amplifier, and finally connected to an Agilent

N5242A PNA-X network analyzer used as multi-frequency generator. The choice of the power amplifier is crucial as will be discussed in section IV. As we are dealing with nonlinear phenomena, varying power levels must be considered. Instead of varying the power level we may make the distance between the transmitter and the DUT variable, where the lower bound of that distance must still respect the far-field condition. In the sequel, the in-the-band frequency range is defined by its lower f_L and its upper frequency f_H. In our experiments we focus on the ISM-band extending from 2.4 GHz up to 2.4835 GHz, but for the ease of the discussion we choose $f_L = 2.4$ GHz to be the lower bound and $f_H = 2.5$ GHz to be the upper bound of the frequency band of interest.

In the remaining part of this chapter, by way of example, we will illustrate the aforementioned strategy to model and test the three different IM distortion scenarios by considering a simple susceptible passive component, combined with a simple active component that causes IMD. The DUT (Fig. 2.6) we consider is an active textile antenna [8] where the susceptible component is the passive antenna, and the active component is a low-noise amplifier (LNA). This example is of practical importance since in many such designs the presence of a frequency selective filter placed between the antenna and the LNA is omitted to reduce cost and to obtain a more compact and more efficient device. The LNA is directly fed by the antenna signal through a via without any matching network [8], choosing as antenna impedance the optimal impedance $(35.05 - j17.644)\Omega$ for minimum noise figure [8]. No filtering operation is provided by intermediate stages in the DUT.

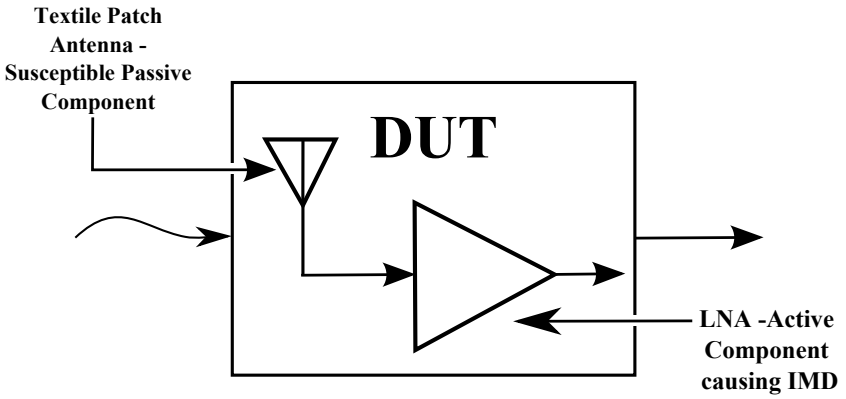

Figure 2.6: Passive antenna and LNA.

In the next section, we first consider the EMC aware design and precompliance testing phase, which focusses on the behavior of the LNA as a stand-alone subsystem/module. The final compliance testing of the complete DUT, being the active antenna, is discussed in Section 2.4.

2.3 EMC Aware Design and Precompliance Testing of the LNA

In contrast to the compliance testing phase, during EMC aware design and precompliance testing, the design engineers have the possibility to model, measure and manipulate the generation and propagation of IM products in isolated subsystems and modules. Hence, including IM distortion in the EMC aware design and precompliance testing cycles offers a cheap and efficient way to avoid in-the-band leakage of undesired signals in the final product. Let us now discuss our strategy by focussing on the LNA module of the active antenna. Models and measurements in this section are based on an LNA that is terminated by 50 Ω at both input and output ports.

Low-noise amplifiers are traditionally characterized by their OIP3, OIP2 and P_{1dB} levels. Table 2.1 compares the results obtained through simulations with Agilent's Advanced Design System (ADS) to the values measured with the Agilent N5242A PNA-X Network Analyzer at 2.45 GHz. A good agreement is obtained between simulated and measured data. However, the interpretation of these numbers requires awareness of the specific modeling/measurement setup that led to each of these results. We note that P_{1dB} was obtained by injecting a single tone at 2.45GHz, whereas two in-the-band tones spaced by 10 MHz and centered around 2.45 GHz were injected to find OIP3. Yet, to study OIP2, a single tone, now at 1.225GHz, is again considered, observing the circuit's response at 2.45 GHz. In a real situation, the input power levels will never be that high as to e.g. reach the third order interception point. Furthermore, the actual nonlinear circuit will exhibit a frequency-dependent behavior, given that all components possess frequency-dependent characteristics, specifically when considering the effect of unwanted out-of-band components that may be present in a very wide frequency band, much wider than intended by the design engineer. Hence, in EMC aware design and testing, we must carefully analyze the problem for different tone spacings and power levels.

Therefore, to characterize the effect of out-of-band signals, the Spurious Free Dynamic Range (SFDR) is put forward as a suitable measure. In literature [9, 10] several definitions of the SFDR can be found. For our purposes, we define SFDR as the ratio between the desired component and the highest spurious one leaking into the band(s) of operation, as schematically shown in Fig.2.7. In EMC aware design an upper limit for this SFDR should be set and modelled/tested for different combinations of desired and/or unwanted signals. In this chapter, by way of example, we will consider a spurious component to be acceptable as long as the SFDR is higher than 40 dB. However, it must be kept in mind that the optimum threshold is strictly application-dependent.

We first discuss the relevancy in terms of EMC aware design of the modelling / measurement data that led to the results of Table 2.1. These data are the gain at 2.45 GHz, the SFDR for two tones centered at 2.45 GHz ($f_1 = 2.445$ GHz and $f_2 = 2.455$ GHz) and the power of the second-order harmonic modelled/measured for varying power

levels, as shown in Fig. 2.8. A good agreement is found between simulated and measured gain and for the power of the second-order harmonic but less so for the SFDR. The SFDR results refer to the ratio between the in-the-band tone and the highest in-the-band intermodulation product. The measured SFDR value stays above 40 dB for an input power lower than -3 dBm. For the sake of completeness, P_{NF} (Power Noise Floor) and P_{MDS} (Power Minimum Detectable Signal) were also measured by means of the Agilent N5242A PNA-X Network Analyzer and turn out to be equal to -90 dBm and -52 dBm, respectively.

Although the gain plot demonstrates desensitization at higher input levels, this result is not relevant for our purposes as it is only caused by in-the-band signals. Hence, extra filtering will not affect this curve. In the same way, the SFDR result, produced by two in-the-band components, will not change when introducing filters before the nonlinear component. Hence, for an EMC engineer studying in-the band leakage of undesired components, only data related to the second-order harmonic offers relevant information. To that end an SFDR must be introduced comparing the power of the second-order harmonic leaking into the band to the typical power levels of the desired signals encountered in the application.

Therefore, we now focus on two tones' excitations that typically result in important in-the-band leakage when omitting a filter before the nonlinear component. The first regions that require our attention are the boundaries of the frequency band(s) of operation. Fig. 2.9 shows the output spectrum of the LNA when excited with two tones: in the top figure these tones are located at $f_2 = 2.395$ GHz and $f_1 = 2.405$ GHz , (i.e. a spacing of 10 MHz centered at the lower end of the ISM band), whereas in the bottom figure the two tones are centered around the upper bound of the band, at $f_1 = 2.495$ GHz and $f_2 = 2.505$ GHz. The values given in Fig. 2.9 are for an input power level of $P_{in} = P_{1dB}$, with $P_{1dB} = -0.498$ dBm (see Table I). This high input power level was deliberately selected in order to obtain the worst case results. The results of Fig. 2.9 clearly show the existence of unwanted in-the-band tones. However, the SFDR remains above 40 dB ($+43.54$ dB).

Table 2.1: Main tones power, OIP3, OIP2 measured and simulated.

Value	Simulated [dBm]	Measured [dBm]
$P_{1dB}@f_0 = 2.45$ GHz	-0.601	-0.498
OIP3@$f_1 = 2.445$ GHz, $f_2 = 2.455$ GHz	$+27.76$	$+25.526$
OIP2@$f_0 = 1.225$ GHz	$+72.394$	$+61.763$

Next, the power level of the out-of-band tone is kept at P_{1dB} but the in-the-band tone power level is decreased to -10 dBm. This is considered to be relevant for the test phase because in a real transmission context it is very likely that an out-of-band component can be stronger in power than the in-the-band one. The obtained results

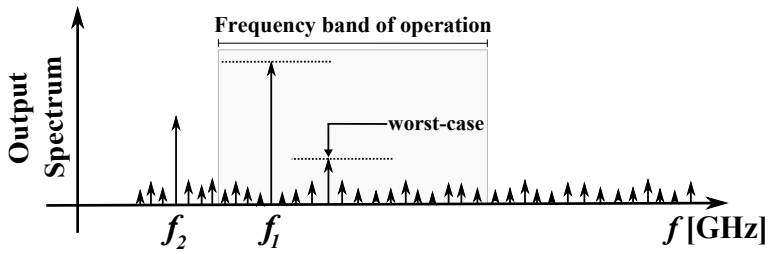

Figure 2.7: Worst-case identification for the calculation of the Spurious Free Dynamic Range.

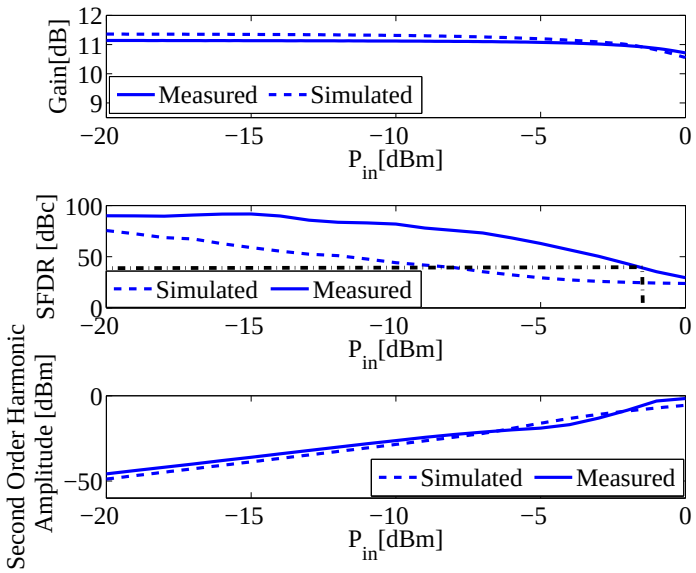

Figure 2.8: Gain at $f_0 = 2.45$ GHz, SFDR for $f_1 = 2.445$ GHz and $f_2 = 2.455$ GHz, and second-order harmonic power for $f_0 = 1.225$ GHz, simulated and measured.

are shown in Fig. 2.10. We observe a difference of 59.35 dB between the in-the-band tone and the highest spurious component falling within the band. Hence, the SFDR is again acceptable. Besides these example configurations, other two-tone excitations, even two out-of-band signals, may result in relevant in-the-band leakage. However, filtering thanks to the frequency dependency of the susceptible linear component may reduce the power of these leaking IM products, as discussed in the next section.

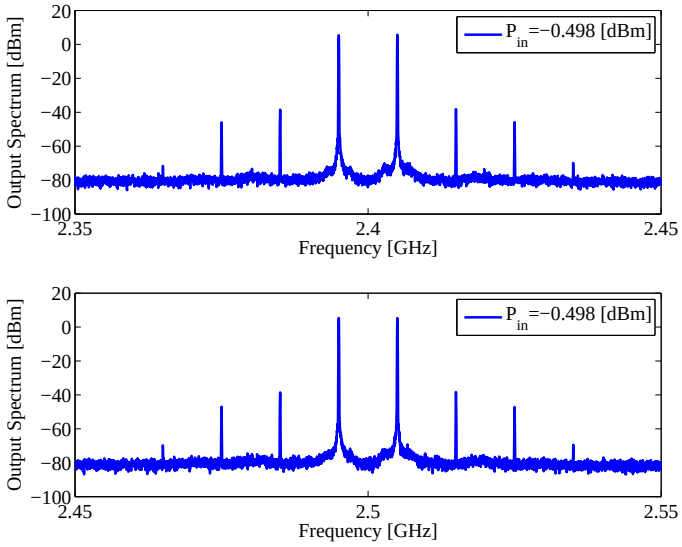

Figure 2.9: Output spectrum with $P_{in} = P_{1dB}$ at the lower and at the upper side of the considered frequency band, for Δf = 10 MHz and excitation by two equal power tones f_1 and f_2.

2.4 Compliance Testing of the Active Antenna

Let us now turn to the compliance testing phase of the DUT (Fig. 2.11), in which all relevant scenarios leading to in-the-band leakage should be verified. To generate a strong enough incident signal, two highly linear power amplifiers are cascaded: the highly linear power amplifier contained in the Agilent N5242A PNA-X Network Analyzer and a $Mini-Circuits\ ZRL-3500$ power amplifier providing a maximum gain of $G_{PA} = 21$ dB. The choice for that type of amplifier is not arbitrary. Indeed, we must make sure that its linearity is superior to that of the LNA which is part of our DUT. If this would not be the case, our test set-up would indeed not make sense. This makes clear that the choice for a particular additional amplifier in the measurement chain depends on the specific DUT one is interested in. The $Mini-Circuits\ ZRL-3500$ power amplifier (further refered to as MC amplifier) has an OIP3 of $+45$ dBm. The maximum allowed input power is specified to be $+10$ dBm. However, when using the MC amplifier in a cascade with the PNA-X amplifier, careful experiments have revealed that this input power must be further restricted in order to drive the second amplification stage without generating IMD, distortion which could perturb the measurement results of the DUT. Several tests were performed to characterize the amplifier cascade in terms of linearity, by driving the input of the MC amplifier with a

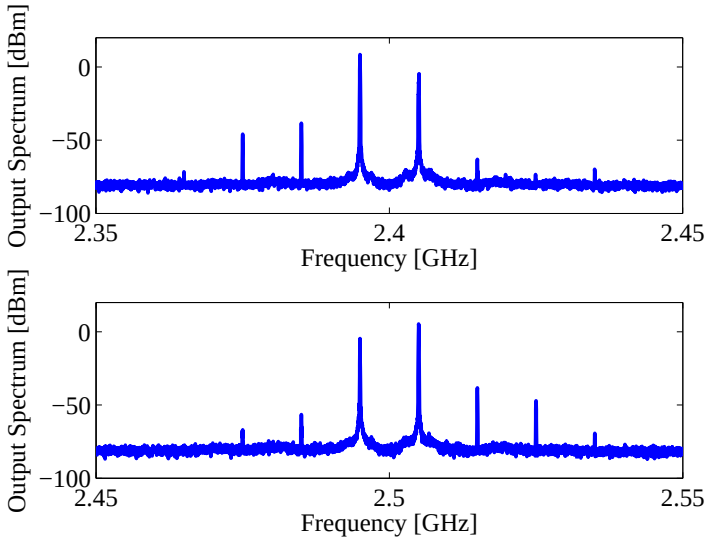

Figure 2.10: Measurement results as in Fig. 2.9 but now for two tones with a power difference of 10 dBm.

variable power (emitted by the PNA-X) ranging from -20 to 0 dBm. Up to 0 dBm no significant IMD turns up and hence this 0 dBm will be the highest input power level at the MC amplifier used for the DUT measurements. To define the relevant power range of desired and unwanted signals incident from the standard gain horn onto the DUT we rely on the Equivalent Isotropically Radiated Power (EIRP) [11], being the amount of power that the standard gain horn emits to produce the peak power density in the direction of maximum antenna gain. Referring to Fig. 2.11, the EIRP is given by :

$$\begin{aligned} EIRP\ [\text{dBm}] = P_{[PNA-X]}\ [\text{dBm}] + G_{PA}\ [\text{dB}] \\ +G_{HORN}\ [\text{dBi}] - L_{[cables]}\ [\text{dB}] - M_t\ [\text{dB}], \end{aligned} \tag{2.1}$$

with G_{HORN} the gain of the standard gain horn (Scientific Atlanta SGH-1.1 or 1.7, depending on the desired excitation frequency), L_{cables} the cable losses and with M_t representing the transmission mismatch. The relevant parameters to the measurements at 2.45 GHz are summarized in Table 2.2. We must also take into account that the maximum allowed EIRP that may be radiated by emitters in the 2.45 GHz ISM band is limited in Europe to $+20$ dBm by ETSI EN 300 328 and by the US FCC Rules, Part 15.247, to +36 dBm.

The EIRP is related to the signal at the output of the active textile antenna by

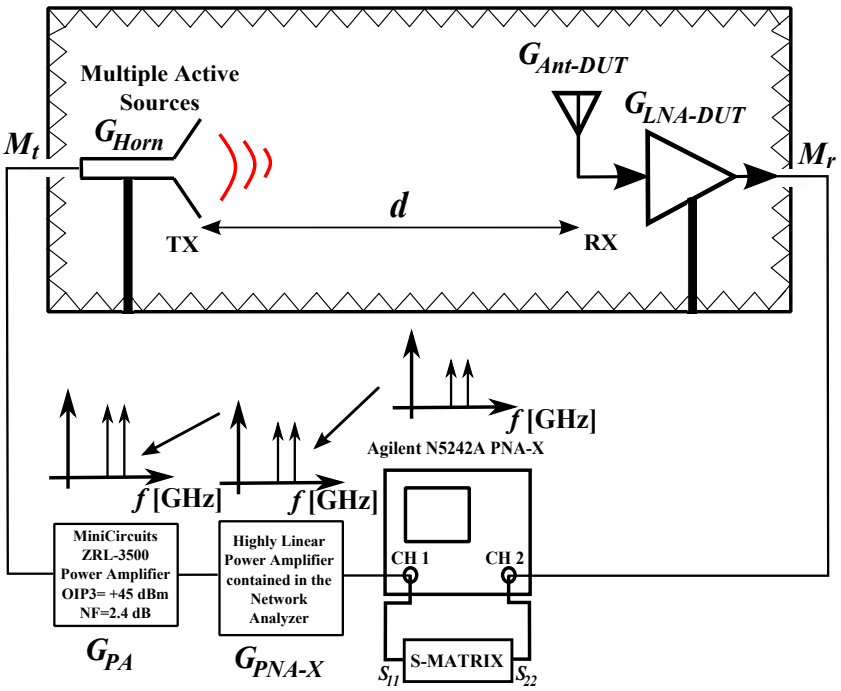

Figure 2.11: DUT measurement setup in the anechoic chamber.

Table 2.2: Relevant parameters to the measurements at 2.45 GHz

$P_{[PNA-X]}$	$G_{[PA]}$	$G_{[HORN]}$	M_t [dB]
-20:1:0 [dBm]	21 [dB]	15.35 [dBi]	-0.1016
$L_{[cables]}$	$G_{[LNA]}$	$G_{[antDUT]}$	M_r [dB]
-0.06 [dB]	+11 [dB]	+3.5 [dBi]	-0.2174

means of

$$P_{\text{out}}[\text{dBm}] = EIRP[\text{dBm}] - PL[\text{dB}] + G_{DUT} - M_r[\text{dB}], \tag{2.2}$$

with PL[dB] the path loss, depending on the distance d between SGA and DUT (Fig. 2.11), M_r the mismatch factor at the receiver and G_{DUT}[dB] $= G_{AntDUT} \times G_{LNA}$ the gain of the complete DUT. G_{DUT} is the product of G_{AntDUT}, the gain of the passive susceptible device, and G_{LNA}, the transducer gain of the nonlinear component with the antenna as its source. Although (2.2) relates to the linear behavior of the DUT, the generation of IM products is directly related to the output level of the DUT. Hence, the IM distortion will be influenced by the frequency selectivity of the path loss and, more importantly, by G_{DUT}. Therefore, it is important to first characterize the gain of

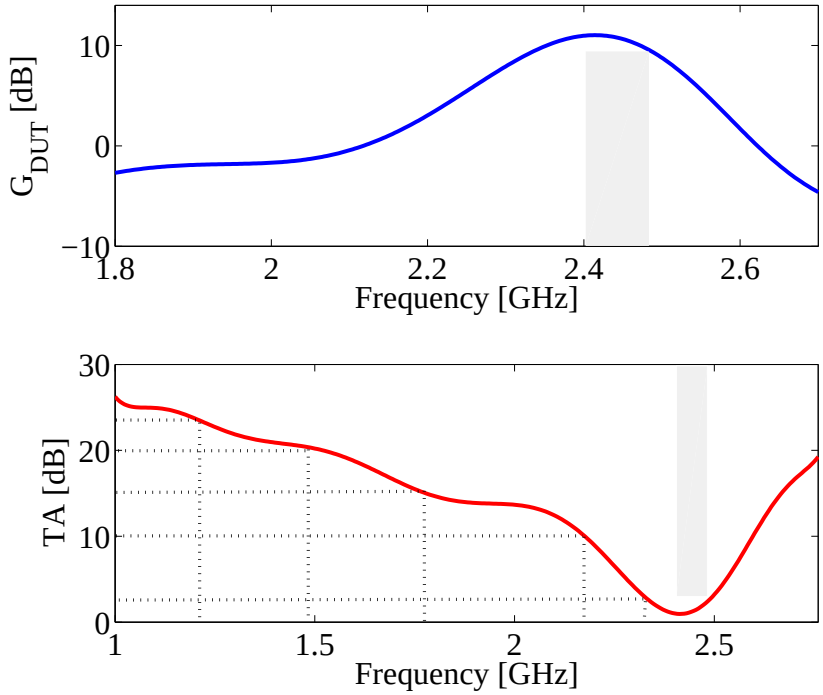

Figure 2.12: G_{DUT} and TA as a function of frequency, with $d = 10\lambda_1$.

the DUT as a function of frequency through a separate S-parameter measurement, by

$$\begin{aligned} G_{DUT}\ [\text{dB}] = S_{21meas}\ [\text{dB}] - M_r\ [\text{dB}] - M_t\ [\text{dB}] \\ +G_{PA}\ [\text{dB}] + G_{HORN}\ [\text{dBi}] - PL[\text{dB}] \end{aligned} \tag{2.3}$$

S_{21meas} represents the measured forward transmission coefficient. The top graph of Fig. 2.12 shows the measured G_{DUT} as a function of frequency. To characterize the effects of frequency-selective gain, we define the Transmission Attenuation (TA) as the absolute value of the difference between the maximum value of G_{DUT} and G_{DUT} as a function of frequency. The resulting TA is shown in the bottom graph of Fig. 2.12. For these measurements we took the distance d to be $10\lambda_1$, with λ_1 the wavelength at 2.45 GHz. We observe that the DUT already provides 3 dB of attenuation at 2.385 GHz and 2.5 GHz, 10 dB at 2.2 GHz and 2.6 GHz. As proposed in Section II, we now investigate the behaviour of the DUT using the three proposed scenarios.

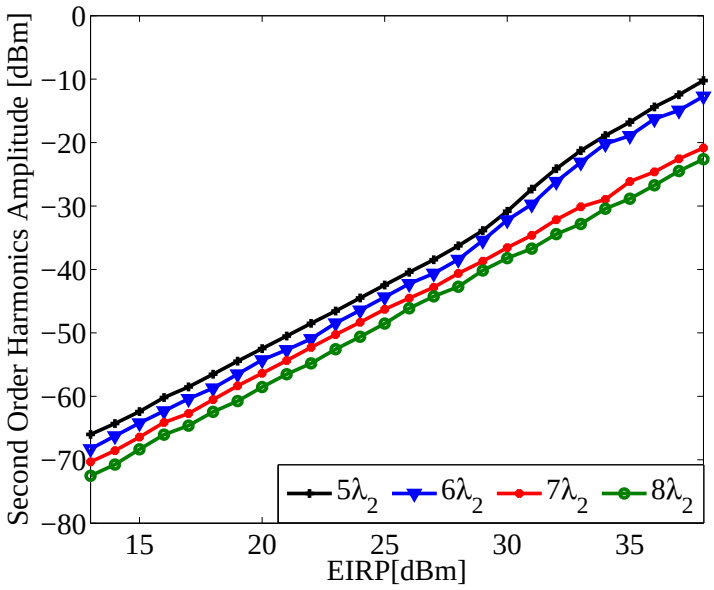

Figure 2.13: Second harmonic's power versus distance d between the standard horn and the DUT.

First Scenario (Fig. 2.2)

In our measurement, $f_0 = 1.225$ GHz was used and while sweeping the input power we observe the occurrence of an in-the-band harmonic at $2f_0$= 2.45 GHz. The test was performed for different distances between the standard gain horn and the DUT. Fig. 2.13 shows the second-order harmonic's power over a range of distances from 8 down to $5\lambda_2$ (where λ_2 is the free-space wavelength at 1.225 GHz). The power of the second-order harmonic remains smaller than -52.47 dBm with $d = 5\lambda_2$ for an EIRP of $+20$ dBm. To reach an SFDR of 40dB i.e. our proposed threshold limit, the desired signal at the output of the DUT should reach at least -12.47 dBm for the DUT to pass this EMC test.

Second Scenario (Fig. 2.3)

The two tones radiated by the horn in our experiment are $f_2 = 2.395$ GHz and $f_1 = 2.405$ GHz, with, as for the LNA testing, a spacing of 10 MHz. They have the same power. The EIRP used for the experiments was varied from a minimum of $+10$ dBm up to $+37$ dBm. The distance between horn and DUT was varied from 9 to 12 λ_1 (free-space wavelength at 2.45 GHz). The results shown in Fig. 2.14 and in Fig. 2.15 refer to a distance of $9\lambda_1$ and EIRP levels of $+27, +30, +32$ and $+34$ dBm. For an

EIRP of $+20$ dBm the intermodulation products just reach the noise floor (-90 dBm) and the level of the main tones is -27.31 dBm. In Fig. 2.16, SFDR values are reported which rely on the measurements performed at different distances between the standard gain horn and the DUT. Considering an SFDR threshold of 40 dB, and depending on the distance between the radiating element and the DUT, we can state that the SFDR stays above the threshold for EIRP values smaller than 30 dBm and for a distance larger than $9\lambda_1$.

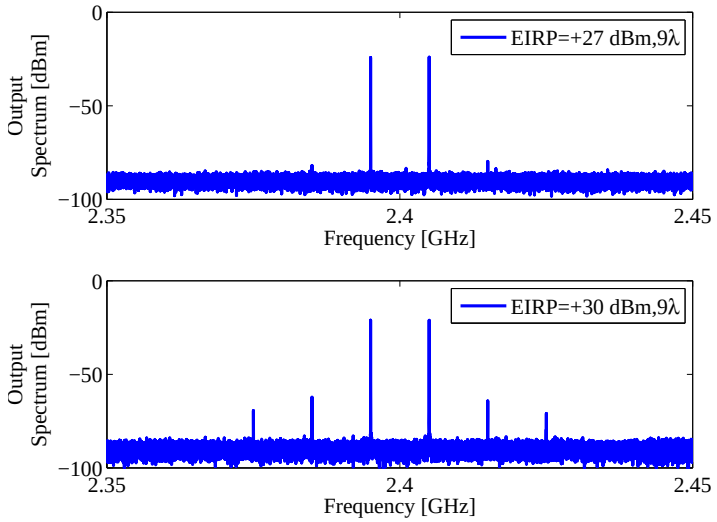

Figure 2.14: Output spectrum for the excitation by two equal power tones in the proximity of the lower side of the frequency band with EIRP=$+27$ dBm and $+30$ dBm respectively, using $d = 9\lambda_1$.

Table 2.3: Largest in-the-band main tone $P_{Tone,1}$ and third-order intermodulation product $P_{Tone,3}$ for varying EIRP values, at a distance $d = 9\lambda_1$.

$EIRP$ [dBm]	$P_{Tone,1}$ [dBm]	$P_{Tone,3}$ [dBm]	SFDR [dB]
+20	-27.3	Noise floor	62.7
+27	-24.2	-79.8	55.6
+30	-21.2	-67.2	46.0
+32	-19.6	-49.0	39.4
+34	-18.3	-39.7	21.4

Similar results are obtained at the upper side of the frequency band and for other distances. Table 2.3 summarizes the power level of the largest in-the-band main tone $P_{Tone,_1}$ and of the strongest in-the-band third-order intermodulation product $P_{Tone,3}$

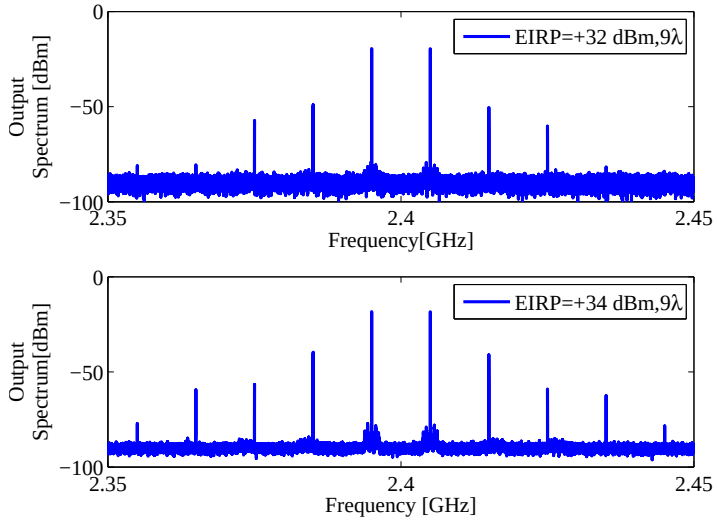

Figure 2.15: Output spectrum for the excitation by two equal power tones in the proximity of the lower side of the frequency band with EIRP=$+32$ dBm and $+34$ dBm respectively, using $d = 9\lambda_1$.

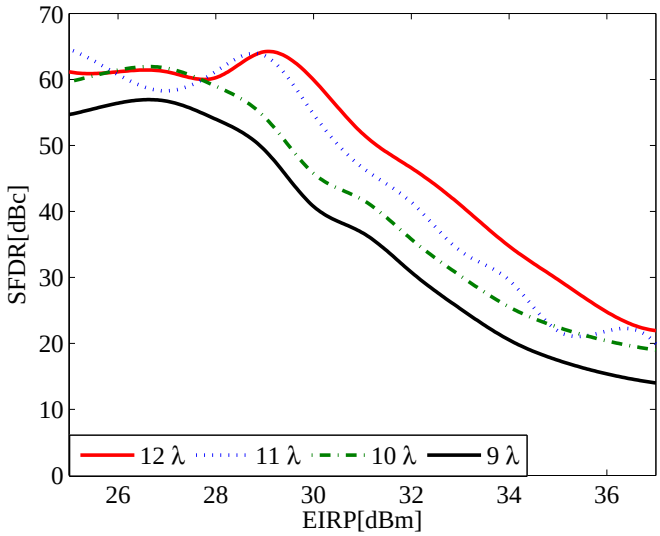

Figure 2.16: SFDR as a function of EIRP for two equal power tones and varying distances ($\lambda = \lambda_1$).

for various EIRP values, at a distance $d = 9\lambda_1$. It is seen that the SFDR drops below 40dB for EIRP$\geq$ 30dBm.

Third Scenario (Fig. 2.4)

Let us now focus on how desensitization affects the SFDR. As already mentioned, any strong undesired signal may reduce the amplification of the desired signal and thereby decrease the SFDR. In most cases, the most critical configuration will be encountered when a strong interfering signal is present near the boundaries of the frequency band of operation, simultaneously causing IM products and desensitization in the DUT. Therefore, again consider the experiment that resulted in Figs. 2.14, 2.15 and 2.16. At the higher EIRP levels we clearly observe that desensitization starts influencing the performance of the DUT. The power of the main tones no longer increases at the same rate as for the lower EIRP values while the intermodulation products grow faster. To characterize this phenomenon an important parameter describing the behavior of the DUT under the variation of EIRP is introduced: the Tone Power Variation TPV_n, defined as

$$TPV_n = \left.\frac{P_{Tone,n}}{EIRP}\right|_{PL=\text{constant}}. \tag{2.4}$$

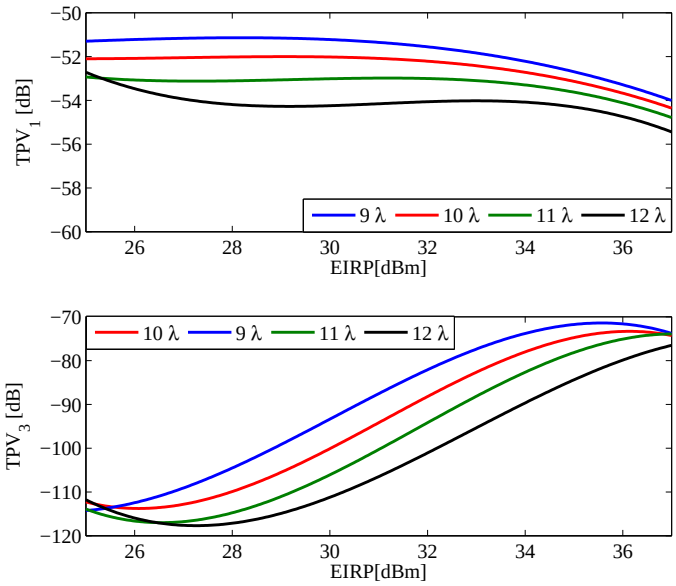

Figure 2.17: TPV_1 and TPV_3 as a function of EIRP and for variable distances $\lambda = \lambda_1$ between horn and DUT.

In Fig. 2.17, TPV_1 and TPV_3 are shown as a function of EIRP, for different distances between transmitter and DUT. In particular, by calculating this variation we can identify the power level at which the amplification starts decreasing, due to the high input power level, for each transmitter-DUT separation. When increasing the EIRP level we expect the power of the main tones to increase by the same quantity and the third-order intermodulation products to grow cubically until the LNA contained in DUT desensitizes due to saturation, exhibiting lower gain, resulting in a higher growth rate for the intermodulation products and in a lower growth for the main tones. This is clearly visible in Fig. 2.17: around $+30$ dBm of EIRP (for the closest distance between the test antenna and the DUT equal to $9\lambda_1$) the LNA starts desensitizing.

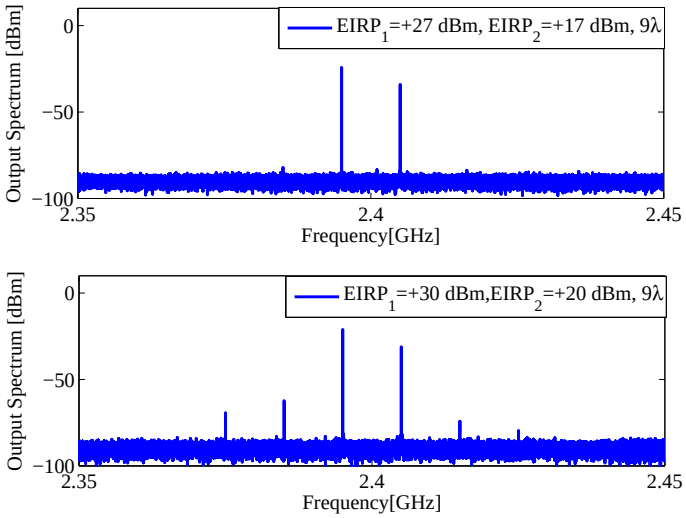

Figure 2.18: Output spectrum for the excitation by two tones with different power in the proximity of the lower side of the frequency band and resp. for $EIRP_1 = 27$ dBm, $EIRP_2 = 17$ dBm and for $EIRP_1 = 30$ dBm, $EIRP_2 = 20$ dBm.

This effect will be even more pronounced when considering a dual-tone co-located transmitter illuminating the DUT, as in the second scenario, but now assuming the out-of-band tone to be much higher in power than the desired signal. In particular, here we choose this unwanted component to be 10 dB higher in power. $EIRP_1$ represents the power level applied to the out-of-band tone, while $EIRP_2$ represents the power level applied to the in-the-band component. In the top part of Fig. 2.18 we observe that the intermodulation products occur at the same level as the noise floor, similar to the case with equal power for the out-of-band and in-the-band component. In Fig. 2.19 we notice that by increasing the $EIRP_1$ to resp. $+32$ dBm and $+34$ dBm, and $EIRP_2$ to resp. $+22$ dBm and $+24$ dBm, the in-the-band intermodulation product

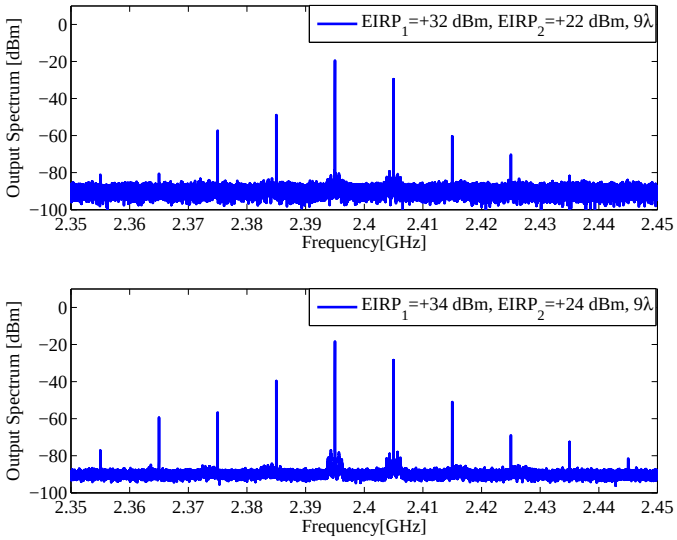

Figure 2.19: Output spectrum for the excitation by two tones with different power in the proximity of the lower side of the frequency band and resp. for $EIRP_1 = 32$ dBm, $EIRP_2 = 22$ dBm and for $EIRP_1 = 34$ dBm, $EIRP_2 = 24$ dBm.

rises to -62.25 dBm and -51.07 dBm, respectively. We observe that the third-order intermodulation product grows faster than cubically due to the influence of the out-of-band component. This phenomenon tends to be more noticeable when increasing the EIRP level. Indeed, for $EIRP_1 = +32$ dBm we observe a difference of 2.39 dB between the expected in-the-band intermodulation product and the measured one. For the case $EIRP_1 = +34$ dBm the difference equals 3.13 dB. This effect quickly reduces the available SFDR. Indeed, for $EIRP_1 = +32$ dBm, the SFDR level equals 30.85 dB, whereas when going to $EIRP_1 = +34$ dBm, the SFDR drops to 18.98 dB.

2.5 Conclusions

Current EMC testing procedures have most often focused on single-source/single-frequency illumination of the devices under test. In general there are no conventional test practices that involve multi-source/multi-frequency testing. Therefore, we have proposed a new modeling and experimental approach dealing with intermodulation distortion phenomena in a transmission context by means of multiple co-located sources. This new approach is suitable for any generic DUT composed of at least one active nonlinear component and a passive susceptible antenna. An active textile antenna (consisting of an LNA and a passive antenna) was used as test bench to prove the

effectiveness of the new approach with the 2.45 GHz ISM-band as the frequency band of interest. By analyzing and measuring the components composing the DUT (in our case the LNA and the passive antenna part) and by subsequently measuring the entire DUT in several transmission scenarios using horn antennas in an anechoic chamber with a PNA-X network analyzer as multi-frequency source, it was shown how a better and more correct knowledge about leakage of undesired signals into the DUT's frequency band of operation when illuminating with a a single out-of-band frequency (scenario 1) or a combination of an in-the-band and an out-of-band frequency (scenario 2) can be obtained. To characterize the effect of harmonics of the out-of-band frequency turning up in the frequency band of interest, the SFDR was put forward as a suitable measure. Furthermore, the influence of strong transmitters, desensitizing the LNA, on the relative importance of intermodulation products in the DUT's output spectrum was carefully examined (scenario 3). As a measure for the desensitization, we introduced the Tone Power Variation parameter, i.e. the ratio of the power of a particular tone to the EIRP of the standard gain horn. For these measurements, an additional highly-linear pre-amplifier (in our case the Mini-Circuits ZRL-3500 power amplifier) was necessary. Concluding, it can be stated that quantitative testing of active DUT's with nonlinear components illuminated by multiple co-located sources emitting both desired, in-the-band, and undesired, out-of-band, signals can be successfully carried out using an anechoic chamber, standard gain horns, a PNA-X network analyzer and a well-chosen linear preamplifier together with a set of clear measurement scenarios.

Bibliography

[1] A. Rembovsky, A. Ashikhmin, V. Kozmin, S. Smolskiy, *Radio Monitoring: Problems, Methods and Equipment*, 1st ed. Springer, 2009.

[2] P. Cruz and K. Remley, "Designing and testing software designed radios," *IEEE Microwave Magazine*, pp. 83–94, Jun. 2010.

[3] I. T. 61000-1-2, "Electromagnetic compatibility (EMC) - part1-2: general-methodology for the achievement of the functional safety of electrical and electronic equipment with regard to electromagnetic phenomena," February 2008. [Online]. Available: http://iec.ch

[4] M. Mardiguian, "Combined effects of several simultaneous, EMI couplings," vol. 1, Washington, August 2000, pp. 181–184.

[5] E. S. J. Nitsch, N. Korovkin and H.-J. Scheibe, "Occurrence of low-frequency noises in electronic systems under action of two-tone high frequency electromagnetic excitation," vol. 2, Magdeburg, Aug. 2005, pp. 618–621.

[6] Duffy, A., Orlandi, A. , Armstrong, K., "Preliminary study of a reverberation chamber method for multiple-source testing using intermodulation," *IET Sci. Meas. Technol.*, vol. 4, pp. 21–27, 2010.

[7] Armstrong, K., "Functional safety requires much more than EMC testing," EMC-Europe, Sept. 2004, pp. 348–353.

[8] F. Declercq and H. Rogier, "Active integrated wearable textile antenna with optimized noise characteristics," *IEEE Trans. Antennas Propag.*, vol. 58, no. 3, pp. 3050–3054, Sep. 2010.

[9] F. Span Application Note, "Spurious Free Dynamic Range." [Online]. Available: http://www.fiber-span.com

[10] E. Lawrence, *RF and Microwave Circuit Design For Wireless Communications*, 1st ed. Artech House, 1997.

[11] C. A. Balanis, *Antenna Theory: Analysis and Design*, 2nd ed. New York: John Wiley & Sons, 1997.

CHAPTER 3

Variability Analysis of Interconnects Terminated by General Nonlinear Loads

Based on the publication:

"Variability Analysis of Interconnects Terminated by General Nonlinear Loads",
IEEE, Transactions on Components Packaging and Manufacturing Technology TCMPT, Special Issue,
Vol. 3, Issue 7, pp. 1244 - 1251 , July 2013

In this chapter, a stochastic modeling method is presented for the analysis of variability effects, induced by the manufacturing process, on interconnect structures terminated by general nonlinear loads. The technique is based on the solution of the pertinent stochastic Telegrapher's equations in time domain by means of the well-established stochastic Galerkin method, but now allows, for the first time in literature, the inclusion of loads with arbitrary I-V-characteristics at the terminals of the lines. The transient solution is obtained by combining the stochastic Galerkin method with a finite-difference time-domain scheme. The proposed technique is validated and illustrated with a meaningful application example, demonstrating its accuracy and efficiency.

3.1 Introduction

The design of electronic systems is becoming increasingly hard because of ever more stringent design specifications, expressed in terms of speed, bandwidth, crosstalk, etc. Moreover, large-scale integration and miniaturization leads to an important impact

of the manufacturing process on the system performance, as this causes uncertainty of the circuit parameters. Therefore, there is a huge need for accurate and efficient stochastic modeling techniques that allow assessing the variability, induced by the manufacturing, during the early design phase [1–3].

On the one hand, the traditional brute-force Monte Carlo (MC) technique can be considered as a robust and reliable stochastic modeling technique. However, for complex systems, the approach is not tractable, as it is known that the convergence of the MC method is slow [4]. Improved techniques, such as quasi-MC techniques [5], have been proposed as well, but unfortunately, their applicability is limited. On the other hand, a class of so-called generalized Polynomial Chaos (gPC) techniques has been developed [6, 7] to efficiently deal with stochastic systems. These techniques turned out to be very useful for the stochastic modeling of electronic circuits and systems [8–12].

The author of this manuscript has especially focussed on stochastic modeling of interconnect structures that are affected by uncertainties in their geometric or material properties [13–15]. Thanks to the application of gPC, a modeling strategy was devised that largely outperformed traditional MC analysis. Unfortunately, as the technique developed in [13–15] is in essence a frequency-domain method, only linear loads, connected to the terminals of the interconnects, could be taken into account. In [10], lumped circuits with nonlinear elements were modeled as well. However, no transmission-line effects were studied, and more importantly, the nonlinearities were described by small-signal analysis or by applying a Taylor expansion around a certain bias point. Hence, all nonlinearities were of a polynomial nature, making the application of gPC again rather straightforward.

In this chapter, we focus on the variability analysis of interconnects that are terminated by general nonlinear loads. The goal is to efficiently and accurately solve the governing stochastic Telegrapher's equations for multiconductor transmission lines (MTLs) and, for this purpose, the well-established Stochastic Galerkin Method (SGM) for MTLs [13–15] is combined with a standard finite-difference time-domain (FDTD) scheme [16]. The approach presented in this chapter, however, allows for the first time in literature, and in contrast to [13–15], the termination of the MTLs by loads that are described by arbitrary I-V-characteristics. It will be shown that these I-V-characteristics can be of a very general nature, even non-smooth, non-polynomial functions can be dealt with. Via numerical integration, an FDTD-update scheme is obtained that requires the solution of a set of nonlinear equations, which can be solved efficiently by providing it with a clever and convenient choice of a seed.

This chapter is organized as follows. In Section 3.2, the proposed formalism is explained starting from the stochastic Telegrapher's equations. The SGM framework is constructed and special attention is devoted to the description of nonlinear loads and to their FDTD implementation. In Section 3.3, the formalism is validated and illustrated by applying it to the variability analysis of a pair of coupled microstrip

lines, terminated by a diode, described by a nonlinear, non-smooth I-V-characteristic. Conclusions are summarized in Section 3.4.

3.2 Stochastic Modeling Formalism and Implementation

3.2.1 Stochastic Telegrapher's Equations

Consider a uniform multiconductor transmission line (MTL) where the axis of invariance is the z-axis. In general, the MTL consists of $\mathcal{N}$ signal conductors and a reference conductor. An example of such a line is given in Fig. 3.1 (Section 3.3), where $\mathcal{N} = 2$. An MTL's behavior is described by the well-known Telegrapher's equations [17]. Often, due to manufacturing, one or more geometrical and/or material parameters are not known in a deterministic way. They have to be treated as stochastic random variables (RVs), characterized by a probability density function (PDF), rendering the Telegrapher's equations nondeterministic. For ease of notation, but without loss of generality, in this section, we consider a single lossless dispersion-free line ($\mathcal{N} = 1$), affected by a single stochastic parameter. (In Section 3.3, an example is given for $\mathcal{N} = 2$ and two stochastic parameters.) We can then write the pertinent *stochastic* Telegrapher's equations as follows:

$$\frac{\partial}{\partial z}\begin{bmatrix} v(z,t,\beta) \\ i(z,t,\beta) \end{bmatrix} = -\begin{bmatrix} 0 & L(\beta) \\ C(\beta) & 0 \end{bmatrix} \cdot \frac{\partial}{\partial t}\begin{bmatrix} v(z,t,\beta) \\ i(z,t,\beta) \end{bmatrix}, \tag{3.1}$$

where v and i are the voltage and current along the line, and with L and C the per-unit-of-length (p.u.l.) transmission line parameters, i.e. the p.u.l. inductance and capacitance respectively. Next to the position z along the line and the time t, we have also explicitly written down the dependence on a stochastic parameter β, of which only the PDF is known, prohibiting a straightforward solution of 3.1. From here on, we denote this PDF of β by $W_\beta(\beta)$, which is defined on a support $\Gamma \subseteq \mathbb{R}$.

3.2.2 Stochastic Galerkin Method (SGM)

To solve the stochastic Telegrapher's equations 3.1, we rely on the so-called Stochastic Galerkin Method (SGM). For a detailed description of this method, applied to transmission lines in the frequency domain, we refer to [13–15]. Here, we repeat the gist of it in the time domain. This will allow us to demonstrate in Section 3.2.3 how the method can be adapted and leveraged to include general nonlinear terminations.

The first step of the SGM is to apply a Polynomial Chaos (PC) expansion, by

rewriting the voltage, current and p.u.l. parameters as follows:

$$v(z,t,\beta) = \sum_{k=0}^{K} v_k(z,t)\phi_k(\beta), \quad L(\beta) = \sum_{k=0}^{K} L_k\phi_k(\beta),$$
$$i(z,t,\beta) = \sum_{k=0}^{K} i_k(z,t)\phi_k(\beta), \quad C(\beta) = \sum_{k=0}^{K} C_k\phi_k(\beta), \tag{3.2}$$

where each function $\phi_k(\beta)$, $k = 0, \ldots, K$, represents a polynomial of degree k. For an efficient expansion, leading to an adequate solution of the stochastic Telegrapher's equations, these polynomials are chosen according to the Wiener-Askey scheme [18], meaning that they are orthogonal w.r.t. to the following inner product:

$$<\phi_k(\beta), \phi_l(\beta)> = \int_\Gamma \phi_k(\beta)\, \phi_l(\beta)\, W_\beta(\beta)\, d\beta = c_k\delta_{kl}. \tag{3.3}$$

In the above equation 3.3, the weighting function $W_\beta(\beta)$ coincides with the PDF of β, and δ_{kl} is the Kronecker delta. The scalar number c_k simply depends on the scaling of the polynomials, e.g., if the polynomials are chosen to be ortho*normal*, then $c_k = 1$, $\forall k = 0, \ldots, K$ [19]. Thanks to the orthogonality, upon knowledge of the p.u.l. parameters L and C as a function of β, the expansion coefficients L_k and C_k, $k = 0, \ldots, K$, are readily computed. The voltage and current expansion coefficients, i.e. v_k and i_k resp., $k = 0, \ldots, K$, are yet unknown.

In the second step of the SGM, the expansions 3.2 are substituted into 3.1 and the result is subjected to a Galerkin testing procedure [20], meaning that the equations are weighted with the same set of polynomials using the inner product 3.3. This leads to the following set of equations:

$$\frac{\partial}{\partial z}\begin{bmatrix} \tilde{\mathbf{v}}(z,t) \\ \tilde{\mathbf{i}}(z,t) \end{bmatrix} = -\begin{bmatrix} 0 & \tilde{\overline{\mathbf{L}}} \\ \tilde{\overline{\mathbf{C}}} & 0 \end{bmatrix} \cdot \frac{\partial}{\partial t}\begin{bmatrix} \tilde{\mathbf{v}}(z,t) \\ \tilde{\mathbf{i}}(z,t) \end{bmatrix}, \tag{3.4}$$

where $\tilde{\mathbf{v}}$ and $\tilde{\mathbf{i}}$ are $(K+1)$-vectors containing the voltage and current expansion coefficients v_k and i_k, and where $\tilde{\overline{\mathbf{L}}}$ and $\tilde{\overline{\mathbf{C}}}$ are $(K+1) \times (K+1)$ matrices, with matrix elements $\tilde{L}_{ml} = \sum_{k=0}^{K} L_k\alpha_{klm}$ and $\tilde{C}_{ml} = \sum_{k=0}^{K} C_k\alpha_{klm}$ where $\alpha_{klm} = <\phi_k(\beta)\phi_l(\beta), \phi_m(\beta)>/c_m$ ($l, m = 0, \ldots, K$). In summary, thanks to the SGM, we have gone from a set of two stochastic equations 3.1 to an augmented set of $2(K+1)$ deterministic equations 3.4. Indeed, in 3.4, the dependency on β has vanished at the cost of an increased number of unknowns, being the voltage and currents expansion coefficients v_k and i_k. Additionally, it is worth mentioning that the augmented equations 3.4 have exactly the same shape as a classical set of Telegrapher's equations for $K+1$ lines, and it has been proven in [19] and [21] that reciprocity and passivity of these "augmented lines" are preserved.

3.2.3 Boundary Conditions (BCs): General Nonlinear Loads

From the above, it can be concluded that upon knowledge of the $2(K+1)$ unknown expansion coefficients v_k and i_k, $k = 0, \ldots, K$, the stochastic problem is fully determined. To find these unknowns, the set of $2(K+1)$ augmented equations 3.4 needs to be solved using standard mathematical methods, and hence, a proper set of $2(K+1)$ boundary conditions (BCs) is required. These BCs evolve from the generators and loads attached to the terminals of the original stochastic line 3.1. It has been explained in [15] that linear loads can easily be dealt with. In this chapter, however, we focus on the inclusion of general nonlinear loads, described by arbitrary I-V-characteristics, within the well-established SGM framework. This opens up a much wider range of applications.

Consider again the single stochastic line, described by 3.1, with a finite length $\mathcal{L}$. We assume that a nonlinear load is attached to the far-end terminal, i.e. at $z = \mathcal{L}$:

$$i(\mathcal{L}, t, \beta) = F(v(\mathcal{L}, t, \beta)), \tag{3.5}$$

where $F(\cdot)$ represents a general nonlinear function. To construct the pertinent BCs, allowing to solve the augmented equations 3.4, we proceed as follows. First, the PC-expansions 3.2 of the voltage and the current at the load are inserted into 3.5:

$$\sum_{k=0}^{K} i_k(\mathcal{L}, t)\phi_k(\beta) = F\left(\sum_{k=0}^{K} v_k(\mathcal{L}, t)\phi_k(\beta)\right). \tag{3.6}$$

Second, 3.6 is Galerkin tested, yielding:

$$\begin{aligned} &\forall m = 0, \ldots, K : \\ &\quad i_m(\mathcal{L}, t) = \frac{1}{c_m} < F\left(\sum_{k=0}^{K} v_k(\mathcal{L}, t)\phi_k(\beta)\right), \phi_m(\beta) > . \end{aligned} \tag{3.7}$$

Note that for linear loads [15] and for loads described by a polynomial function $F(\cdot)$ [10], the inner product in the rhs of 3.7 can be calculated analytically, leading to a simple set of $(K+1)$ BCs for the equations 3.4. Such a set of augmented BCs represents a linear or polynomial relationship between the voltage and current expansion coefficients at the terminal $z = \mathcal{L}$. In contrast, for arbitrary, nonlinear $F(\cdot)$, such an approach is not possible, and therefore, we will now construct an approximate analytical relationship between the current and voltage expansion coefficients at the terminals. Thereto, the integral pertaining to the inner product, is solved numerically, as follows:

$$< F\left(\sum_{k=0}^{K} v_k(\mathcal{L}, t)\phi_k(\beta)\right), \phi_m(\beta) >$$

$$= \int_{\Gamma} F\left(\sum_{k=0}^{K} v_k(\mathcal{L},t)\phi_k(\beta)\right)\phi_m(\beta)\,W_\beta(\beta)\,d\beta$$
$$\approx \sum_{n=1}^{N} w_n\,G_{n,m}(v_0(\mathcal{L},t),\ldots,v_K(\mathcal{L},t),\beta_n), \tag{3.8}$$

with

$$G_{n,m}(v_0(\mathcal{L},t),\ldots,v_K(\mathcal{L},t),\beta_n) = F\left(\sum_{k=0}^{K} v_k(\mathcal{L},t)\phi_k(\beta_n)\right)\phi_m(\beta_n). \tag{3.9}$$

In 3.8, any kind of numerical integration technique can be used, ranging from the classical trapezoidal rule, over Gaussian quadrature rules, to highly adaptive integration schemes [22]. In all these cases, and depending on the desired accuracy, the integration comes down to selecting N nodes β_n in the domain Γ and a corresponding set of N weights w_n. (Obviously, it is hard to exactly predict the number of nodes that is strictly required for all kinds of nonlinearities that one can encounter. Nonetheless, an illustrative example is given in Section 3.3.) Finally, a set of $(K+1)$ BCs is found, being a set of $K+1$ coupled, nonlinear relations between the voltage and current expansion coefficients at the terminals $z=\mathcal{L}$ of the augmented lines 3.4, as follows:

$$\forall m = 0,\ldots,K:\ i_m(\mathcal{L},t) \approx \tilde{F}_m(v_0(\mathcal{L},t),\ldots,v_K(\mathcal{L},t)), \tag{3.10}$$

or in vector form

$$\tilde{\mathbf{i}}(\mathcal{L},t) \approx \tilde{\mathbf{F}}\left[\tilde{\mathbf{v}}(\mathcal{L},t)\right], \tag{3.11}$$

where, after omitting the argument, the nonlinear functions $\tilde{F}_m$, $m=0,\ldots,K$, contained in the vector of functions $\tilde{\mathbf{F}}$, are given by

$$\tilde{F}_m = \frac{1}{c_m}\sum_{n=1}^{N} w_n\,G_{n,m}. \tag{3.12}$$

Note that in the above expressions the $\approx$-sign was used explicitly to stress that no analytically correct calculation can be obtained, this in contrast to the case where linear or polynomial loads are used. Nevertheless, still a very good accuracy is obtained, as shown in Section 3.3. Obviously, a similar technique can be used at the other terminal $z=0$, leading to a second set of $K+1$ BCs, allowing to solve the $2(K+1)$ equations 3.4.

3.2.4 Implementation via the Finite-Difference Time-Domain (FDTD) Method

To solve the augmented set of equations 3.4 in conjunction with a set of nonlinear BCs such as 3.11, in this chapter we adopt a finite-difference time-domain (FDTD) technique for transmission lines [17]. Of course, as the above formulation to handle nonlinearities is in fact independent from the time-domain solution technique, other methods, such as, e.g., waveform relaxation techniques [23] could be used as well. We now briefly recapitulate the FDTD method for transmission lines. We opt not to dwell on the inclusion of frequency-dependent losses, but rather focus on the implementation of the nonlinear terminations 3.11. For a detailed explanation on FDTD we refer the reader to [16, 17].

The line of length $\mathcal{L}$ is divided into N_z equal sections of length Δz. In a similar fashion, the total simulation time is divided into N_t time segments of length Δt. The voltage waveforms $v_k(z,t)$ along the line are assessed in N_z+1 discrete nodes $z_p = p\Delta z$, $p = 0,\ldots,N_z$, and at times $q\Delta t$, $q = 0,\ldots,N_t$. The current waveforms $i_k(z,t)$ are assessed in N_z discrete nodes $z_p = (p+\frac{1}{2})\Delta z$, $p = 0,\ldots,N_z-1$, and at times $(q+\frac{1}{2})\Delta t$, $q = 0,\ldots,N_t-1$. This interlacing guarantees an accurate FDTD-scheme. The voltage and current variables, discretized in space and time according to this scheme, are contained in $(K+1)$-vectors $\tilde{\mathbf{v}}_p^q$ and $\tilde{\mathbf{i}}_{p+\frac{1}{2}}^{q+\frac{1}{2}}$. After discretization of the Telegrapher's equations 3.4, i.e. after approximating the derivatives $\frac{\partial}{\partial z}$ and $\frac{\partial}{\partial t}$ by finite differences and neglecting second-order terms, the following typical FDTD-leapfrog scheme is obtained:

$$\tilde{\mathbf{v}}_p^{q+1} = \tilde{\mathbf{v}}_p^q - \frac{\Delta t}{\Delta z}\,\tilde{\overline{\mathbf{C}}}^{-1}\cdot\left(\tilde{\mathbf{i}}_{p+\frac{1}{2}}^{q+\frac{1}{2}} - \tilde{\mathbf{i}}_{p-\frac{1}{2}}^{q+\frac{1}{2}}\right), \tag{3.13}$$

$$\tilde{\mathbf{i}}_{p+\frac{1}{2}}^{q+\frac{3}{2}} = \tilde{\mathbf{i}}_{p+\frac{1}{2}}^{q+\frac{1}{2}} - \frac{\Delta t}{\Delta z}\,\tilde{\overline{\mathbf{L}}}^{-1}\cdot\left(\tilde{\mathbf{v}}_{p+1}^{q+1} - \tilde{\mathbf{v}}_p^{q+1}\right). \tag{3.14}$$

The voltages and currents are solved by iterating p for a fixed time (recursively solving first 3.13 and second 3.14), and then iterating time. All voltage and current variables are treated in this way, except for the voltages at the terminals $z = 0$ ($p = 0$) and $z = \mathcal{L}$ ($p = N_z$), for which special update functions need to be constructed. It is readily proven [17] that these are given by:

$$\tilde{\mathbf{v}}_0^{q+1} = \tilde{\mathbf{v}}_0^q - \frac{2\Delta t}{\Delta z}\,\tilde{\overline{\mathbf{C}}}^{-1}\cdot\left(\tilde{\mathbf{i}}_0^{q+\frac{1}{2}} - \tilde{\mathbf{i}}_{\mathrm{ne}}^{q+\frac{1}{2}}\right), \tag{3.15}$$

$$\tilde{\mathbf{v}}_{N_z}^{q+1} = \tilde{\mathbf{v}}_{N_z}^q - \frac{2\Delta t}{\Delta z}\,\tilde{\overline{\mathbf{C}}}^{-1}\cdot\left(\tilde{\mathbf{i}}_{\mathrm{fe}}^{q+\frac{1}{2}} - \tilde{\mathbf{i}}_{N_z-1}^{q+\frac{1}{2}}\right), \tag{3.16}$$

where the vectors $\tilde{\mathbf{i}}_{\mathrm{ne}}^{q+\frac{1}{2}}$ and $\tilde{\mathbf{i}}_{\mathrm{fe}}^{q+\frac{1}{2}}$ contain the $(K+1)$ currents flowing through the terminals at the near-end $z = 0$ and the far-end $z = \mathcal{L}$ respectively. Consider now nonlinear loads at the far-end, described by general nonlinear I-V-characteristics 3.11,

here repeated in discretized form:

$$\tilde{\mathbf{i}}_{\mathrm{fe}}^{q+\frac{1}{2}} \approx \tilde{\mathbf{F}}\left[\tilde{\mathbf{v}}_{N_z}^{q+\frac{1}{2}}\right] \approx \tilde{\mathbf{F}}\left[\frac{1}{2}\left(\tilde{\mathbf{v}}_{N_z}^{q} + \tilde{\mathbf{v}}_{N_z}^{q+1}\right)\right]. \tag{3.17}$$

To update the value of the voltage variables at the terminal, 3.17 is inserted into 3.16 as follows,

$$\tilde{\mathbf{v}}_{N_z}^{q+1} = \tilde{\mathbf{v}}_{N_z}^{q} - \frac{2\Delta t}{\Delta z}\tilde{\overline{\mathbf{C}}}^{-1}\cdot\left(\tilde{\mathbf{F}}\left[\frac{1}{2}\left(\tilde{\mathbf{v}}_{N_z}^{q} + \tilde{\mathbf{v}}_{N_z}^{q+1}\right)\right] - \tilde{\mathbf{i}}_{N_z-1}^{q+\frac{1}{2}}\right), \tag{3.18}$$

and this equation should be solved for $\tilde{\mathbf{v}}_{N_z}^{q+1}$. At the near-end $z = 0$, a similar procedure can be applied, solving for $\tilde{\mathbf{v}}_{0}^{q+1}$. For general nonlinear functions $\tilde{\mathbf{F}}[\cdot]$, often, 3.18 is a transcendental equation. In our work, the FDTD scheme is implemented in Matlab, and the update function 3.18 is handled by making use of the $\mathrm{fsolve.m}$ routine, which allows to find the roots of a set of coupled nonlinear equations. It is interesting to mention that, thanks to the FDTD scheme, we can assure a fast converge of the iterative solution provided by this fsolve-routine. Indeed, to find the update value for $\tilde{\mathbf{v}}_{N_z}^{q+1}$, we seed the solver with the previous voltage $\tilde{\mathbf{v}}_{N_z}^{q}$, which turns out to be an excellent initial value. The discretization step Δz is chosen sufficiently small to properly resolve all wave dynamics. By respecting the Courant condition $\Delta t \leq \frac{\Delta z}{v_{\max}}$, with $v_{\max}$ the speed of the fastest fundamental eigenmode pertaining to the $K+1$ lines, the actual waveform can be reproduced with very good accuracy.

3.3 Numerical Results

In this section, the above outlined technique is validated and illustrated by applying it to the variability analysis of a pair of coupled PEC microstrip lines ($\mathcal{N} = 2$). The cross-section of the lines is given in Fig. 3.1(a), where $w = 100$ μm, $h = 500$ μm and $t = 35$ μm. The gap G between the lines and the relative permittivity ϵ_r of the substrate are considered to be two Gaussian RVs with means $\mu_G = 80$ μm and $\mu_{\epsilon_r} = 4$ respectively, and with normalized standard deviations $\sigma_G = 5\%$ and $\sigma_{\epsilon_r} = 5\%$. As shown in Fig. 3.1(b), the lines are given a length of $\mathcal{L} = 5$ cm. One line, called the active line, is excited by means of a voltage source $v_s(t)$ that produces a ramped step, going from 0 V to 1 V in a risetime of 100 ps. The generator impedance is $R_{g1} = 50\,\Omega$. This active line is terminated by means of a forward biased diode. The diode's I-V-characteristic is given by:

$$i = F(v) = \begin{cases} 0 & , v < v_1 \\ \frac{v-v_1}{R_1} & , v_1 \leq v < v_2 \\ \frac{v-v_2}{R_2} + \frac{v_2-v_1}{R_1} & , v \geq v_2 \end{cases}, \tag{3.19}$$

where $v_1 = 0.67$ V, $v_2 = 0.73$, $R_1 = 1\ \Omega$, and $R_2 = 0.1\ \Omega$. This is a three-line piecewise linear model [24], as shown in Fig. 3.2. This kind of model is chosen for three reasons. First, such a model is often preferred because of the presence of the current-limiting resistor R_2, this in contrast to the well-known Shockley-model $i = I_s \left(e^{\frac{v}{\eta V_t}} - 1 \right)$ with an exponentially increasing current. Second, it allows to show that even non-smooth, complex I-V-characteristics can be treated with great accuracy and efficiency with our technique, which is rather challenging. (For comparison, the smooth Shockley model's I-V-characteristic is also shown on Fig. 3.2, where the typical parameters are $I_s = 5 \cdot 10^{-14}$ A, $\eta = 1$, and $V_t = 25.85$ mV.) Third, the nonlinearity induced by this I-V-characteristic will lead to a clipping of the voltage across the load. Hence, this can be considered as a "hard nonlinearity", in contrast to, e.g., the rather mild distortion introduced by amplifiers working in small-signal regime or by I/O buffers with a very high input impedance. The second line, called the victim line, is terminated at the near-end by means of a $50\ \Omega$ load R_{g2}. At the far-end, a 1 pF ideal capacitor C_L is connected. We are interested in the voltage waveforms v_{in} at the input of the active line, v_{out} at the diode, the near-end crosstalk v_{NX} and the far-end crosstalk v_{FX}, all indicated on Fig. 3.1.

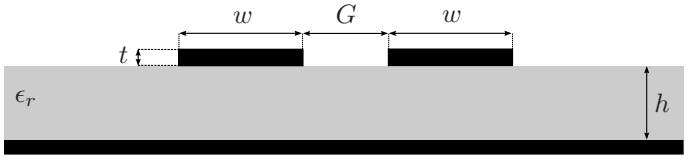

(a) Cross-section AA' of the source-line-load configuration (Fig. 3.1(b)), where $w = 100\ \mu$m, $h = 500\ \mu$m and $t = 35\ \mu$m. The gap G between the lines and the relative permittivity ϵ_r of the substrate are stochastic parameters.

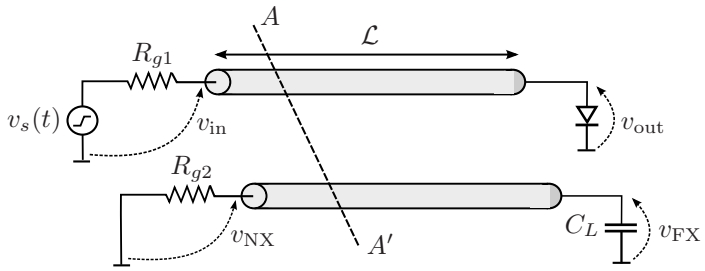

(b) Source-line-load configuration, using cross-section AA' (Fig. 3.1(a)), where $\mathcal{L} = 5$ cm, $v_s(t)$ is a ramped voltage step, $R_{g1} = R_{g2} = 50\ \Omega$, $C_L = 1$ pF, and the diode's I-V-characteristic is given by 3.19.

Figure 3.1: Pair of coupled microstrip lines under study.

To obtain a reference result, first, a Monte Carlo (MC) simulation was performed using 10000 samples of G and ϵ_r, drawn according to their respective Gaussian distribution. These 10000 FDTD simulations were performed using the following set-

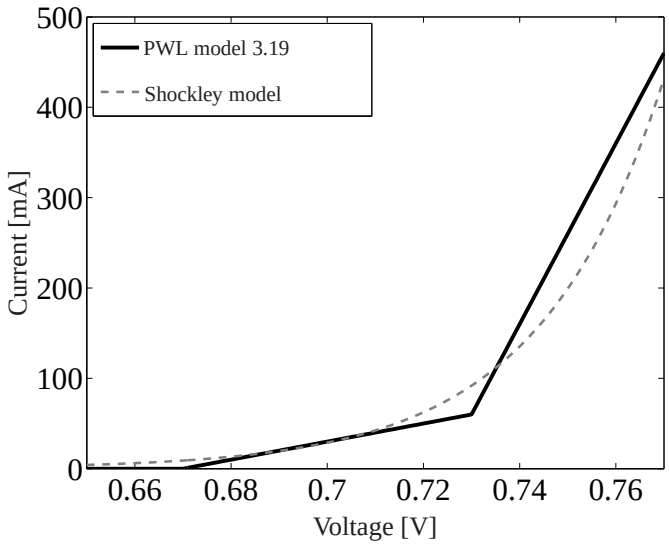

Figure 3.2: Three-line piecewise linear (PWL) diode model according to 3.19. (For comparison, the Shockley model $i = I_s\left(e^{\frac{v}{\eta V_t}} - 1\right)$, with $I_s = 5 \cdot 10^{-14}$ A, $\eta = 1$, and $V_t = 25.85$ mV, is plotted as well.)

tings: $\Delta_t = 0.792$ ps and $\Delta_z = 0.192$ mm. Next, the proposed SGM for nonlinear loads was used. A set of $K + 1 = 10$ orthonormal Hermite polynomials [18] was adopted to model the variability and the numerical integration was performed using 100 cubature points. The FDTD settings were the following: $\Delta_t = 0.842$ ps and $\Delta_z = 0.198$ mm. These SGM-FDTD settings differ slightly from the MC-FDTD settings, because with SGM, actually, an augmented set of $\mathcal{N}(K + 1) = 20$ lines was modeled. This augmented MTL clearly exhibits a different eigenmode behavior than the original set of two lines, used during the MC run, hence a different discretization is needed. In Fig. 3.3 the result is presented. The full black lines indicate the means μ_v of the four voltage waveforms $v_{\rm in}(t)$, $v_{\rm out}(t)$, $v_{\rm NX}(t)$, and $v_{\rm FX}(t)$, at the four terminals of the coupled microstrip lines of Fig. 3.1, and the dashed lines show the $\pm 3\sigma_v$ deviations from these means μ_v, all computed using the SGM-FDTD technique. Thanks to the gPC-representation, the mean and standard deviation of a voltage waveform $v(z, t, G, \epsilon_r)$ are very efficiently calculated as follows [7]:

$$\mu_{v(z,t,G,\epsilon_r)} = v_0(z, t), \tag{3.20}$$

$$\sigma_{v(z,t,G,\epsilon_r)} = \sqrt{\sum_{k=1}^{K} (v_k(z, t))^2}, \tag{3.21}$$

where v_k, $k = 0, \ldots, K$, are the voltage expansion coefficients, obtained by means of

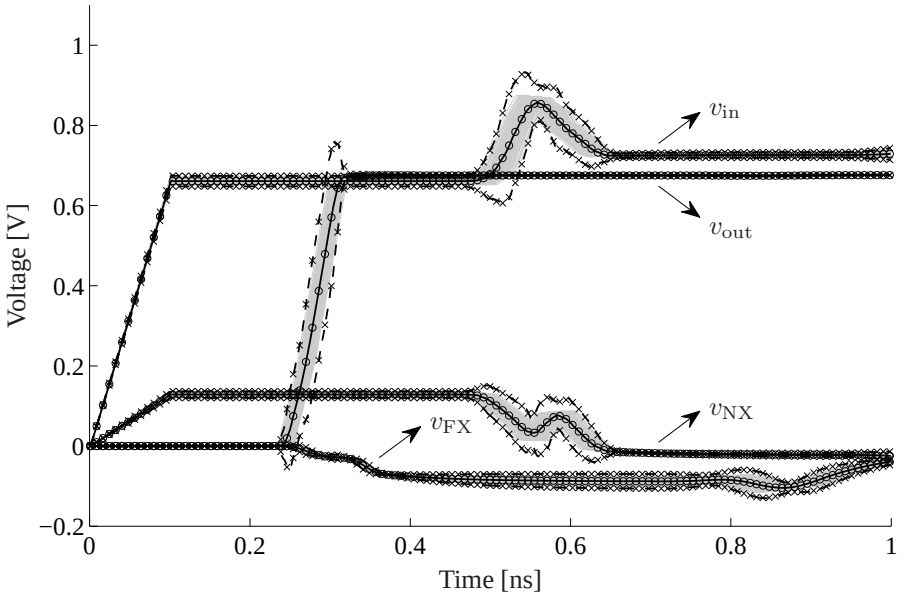

Figure 3.3: Voltage waveforms $v_{\rm in}(t)$, $v_{\rm out}(t)$, $v_{\rm NX}(t)$, and $v_{\rm FX}(t)$, at the four terminals of the coupled microstrip lines of Fig. 3.1. Full black lines: means μ_v computed using the SGM-FDTD technique; Dashed black line: $\pm 3\sigma_v$-variations computed using the SGM-FDTD technique; Circles ($\circ$): means μ_v computed using the MC technique; Crosses ($\times$): $\pm 3\sigma_v$-variations computed using the MC technique; Gray lines: 100 MC samples.

the SGM-FDTD. The gray lines on Fig. 3.3 correspond to 100 samples of the MC run; the circles ($\circ$) and crosses ($\times$) indicate the mean μ_v and the $\pm 3\sigma_v$ deviations, resp., computed using the 10000 samples of the MC run. Apart from the hard nonlinearity induced by the diode, an excellent correspondence between the SGM results and the MC results is observed. Moreover, such graphs can be computed in a very efficient way now. Indeed, whereas the total run time for this MC analysis was 53582 s, the SGM simulation only took 75 s. So, an impressive speed-up factor of 714 is obtained by means of the newly proposed technique. All computations have been performed on a Dell Precision M4500 laptop with an Intel(R) Core(TM) i7 X940 CPU running at 2.13 GHz and 8 GB of RAM.

At this point, it is instructive to comment on the convergence of the MC method. One might argue that 10000 samples seems a lot for this kind of example, but in fact, it is not. In Fig. 3.4 the relative error on the computed mean and variance of the maximum of the far-end crosstalk $\max_{t\geq 0}|v_{\rm FX}(t)|$ is shown as a function of $N_{\rm MC}$, i.e. the number of MC samples used. The mean and variance of $\max_{t\geq 0}|v_{\rm FX}(t)|$, obtained by using all 10000 samples, are 0.10759 V and $1.2552{\cdot}10^{-5}$ V^2 respectively. These values are used as the reference result to compute the relative errors, shown in Fig. 3.4.

As expected, a $1/\sqrt{N_{\mathrm{MC}}}$-convergence rate is obtained. It is also observed that although using 1000 or 2000 samples might be sufficient to obtain a good estimate of the mean, it is not sufficient to get a an accurate result for the variance. The relative error just drops below 1% when 10000 samples are used. In the signal integrity applications we have in mind, it is not sufficient to know the mean value of the crosstalk. Typically, one is interested in the maximum value. To obtain higher-order stochastic moments with sufficient accuracy or to reconstruct the cumulative distribution function (see below), a large number of MC samples is needed. In this perspective, the speed-up factor presented above is not exaggerated and it is safe to state that also for larger examples (with more RVs), still a considerable speed-up w.r.t. MC simulations will be obtained.

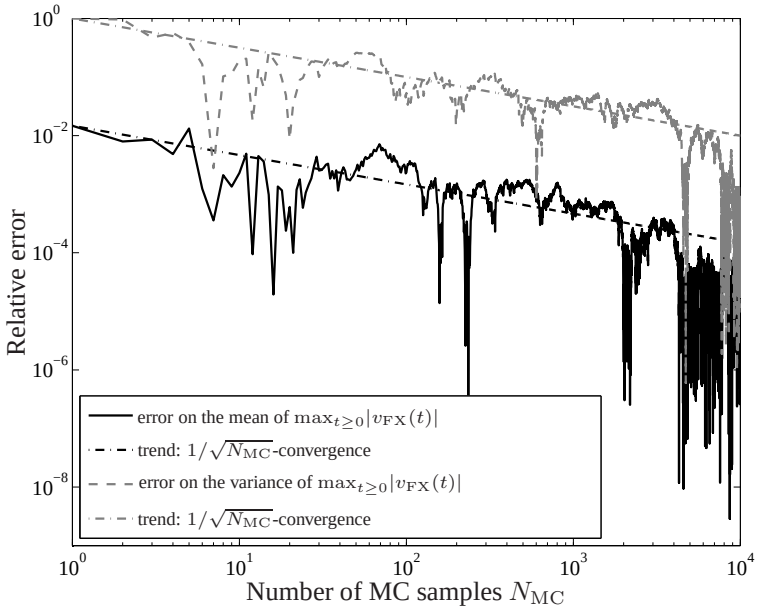

Figure 3.4: Convergence of the MC simulation: relative error on the computed mean and variance of the maximum far-end crosstalk, as a function of the number of MC samples used.

As stated above, a designer is typically interested in the maximum amount of crosstalk he/she can expect. Therefore, in a post-processing step, we compute the cumulative distribution function (CDF) of the maximum of the near-end and far-end crosstalk, i.e. we compute the CDFs of $\max_{t\geq 0}|v_{\mathrm{NX}}(t)|$ and $\max_{t\geq 0}|v_{\mathrm{FX}}(t)|$, using standard analytical or numerical techniques [25]. The results are shown in Figs. 3.5 and 3.6. Although the number of MC samples was still not extremely high, again a good agreement between MC and the SGM-FDTD technique is obtained. From these figures, it is easy to estimate the maximum crosstalk levels that one can expect, or alternatively, it is now readily seen that, e.g., there is an 80% chance that the crosstalk

will take a value less than or equal to 131 mV at the near-end terminal and 110 mV at the far-end terminal.

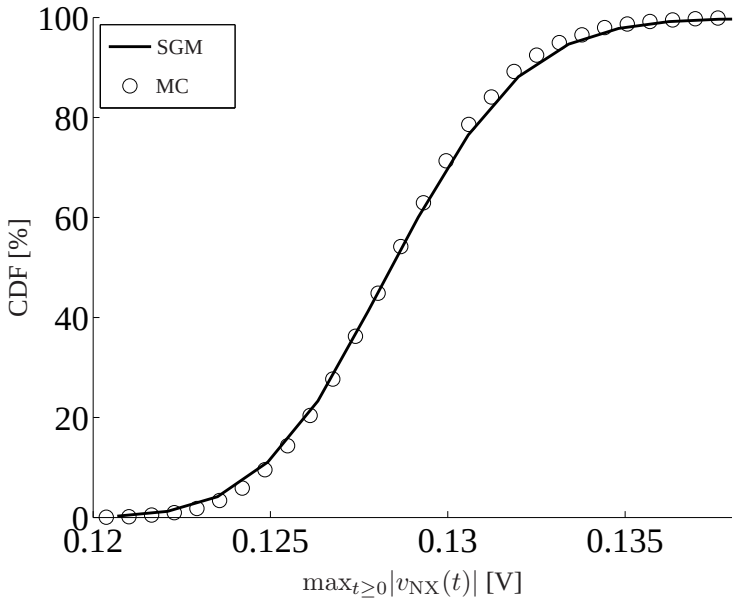

Figure 3.5: Cumulative distribution function (CDF) of the maximum of the near-end crosstalk as presented in Fig. 3.3.

To obtain the above results, we opted to use a Gauss-Hermite cubature integration scheme [26] to compute the inner products 3.8. This is a logical choice for this integral, since the weighting function in the integrand represents a probability density function pertaining to the two independent Gaussian RVs G and ϵ_r. The influence of the number of cubature points, used in the two-dimensional domain Γ, is indicated in Table 3.1. In this table, we present the mean and the variance of $\max_{t\geq 0}|v_{\mathrm{FX}}(t)|$, computed by the 10000 MC samples on the one hand and by the SGM-FDTD method on the other. When the number of cubature points increases to about 10×10, the relative error of SGM-FDTD, compared to MC, drops to the levels that we can expect from Fig. 3.4, i.e. two digits of accuracy on the variance and four digits of accuracy on the mean. All results presented above were obtained with this 10×10 cubature scheme.

3.4 Conclusions

Due to very stringent design specifications, the design of interconnects has become a challenging task. Moreover, the manufacturing process causes geometrical and ma-

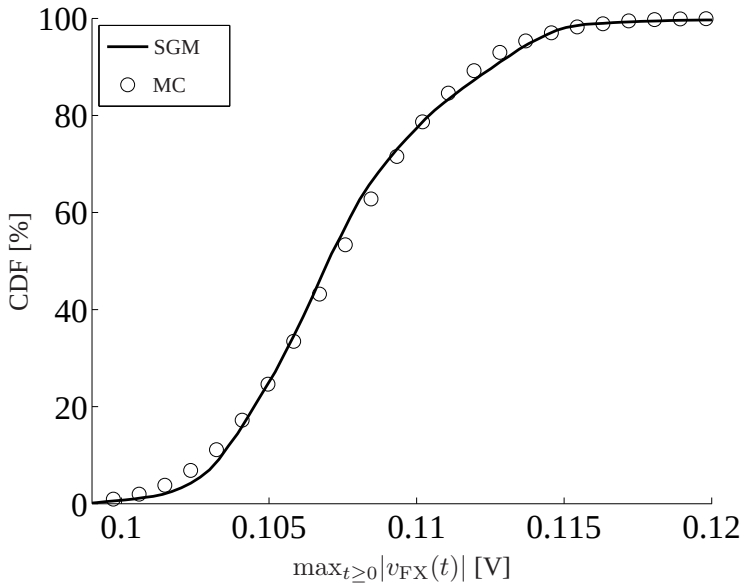

Figure 3.6: Cumulative distribution function (CDF) of the maximum of the far-end crosstalk as presented in Fig. 3.3.

Technique (cubature points)	$\max_{t\geq 0}\|v_{\mathrm{FX}}(t)\|$ mean [V]	variance [V^2]	Relative error [%] mean	variance
MC (10^4 samples)	0.10759	$1.2552\cdot 10^{-5}$	0	0
SGM (1×1)	0.13496	$1.8519\cdot 10^{-2}$	25.4	$>10^6$
SGM (2×2)	0.10853	$6.5588\cdot 10^{-5}$	0.871	423
SGM (5×5)	0.10764	$1.3088\cdot 10^{-5}$	0.0438	4.27
SGM (10×10)	0.10761	$1.2473\cdot 10^{-5}$	0.0179	0.634

Table 3.1: Influence of the number of cubature points (indicated between brackets) in the two-dimensional domain Γ, used in the computation of the inner products 3.8, on the mean and the variance of the maximum of the far-end crosstalk. The relative accuracy w.r.t. the MC run with 10000 samples is also indicated.

terial parameter uncertainties, necessitating the development of stochastic modeling tools that allow assessing the variability effects. In recent literature, polynomial chaos (PC) based techniques have been developed for lumped circuits and distributed interconnects, proving their ability for accurate and efficient variability analysis. However, so far, stochastic interconnect structures could only be terminated by linear loads and PC-based techniques for stochastic lumped circuits could only take mild nonlinearities, described by polynomial I-V-characteristics, into account. Therefore, in this chapter, we solve the stochastic Telegrapher's equations for multiconductor transmission lines (MTLs), by combining the well-established stochastic Galerkin method (SGM) with a finite-difference time-domain (FDTD) scheme. The novelty of this chapter lies in the fact that the SGM-FDTD framework is adapted and leveraged for the first time to also include general nonlinear loads, described by arbitrary I-V-characteristics, at the terminals of the MTL. This opens up a much wider range of applications that can now be tackled. The technique was validated and illustrated by means of an application example, consisting of a pair of coupled microstrip lines exhibiting variability of its geometrical and material parameters, and terminated by a diode with a non-smooth I-V-characteristic. Compared to a standard, robust Monte Carlo analysis, the method shows excellent agreement and far superior efficiency.

Future research will focus on the inclusion of (behavioral models of) *dynamic* nonlinear terminations [27], as well as on the extension of the application examples to I/O bus structures with many random variables. With respect to the latter extension, the scalability of the SGM becomes an important issue. This has also already been adressed in [13, 14]. Also, a comparison with a non-intrusive stochastic modeling technique, such as the stochastic collocation method (SCM) [28], might be useful, as the SCM is more parallelizable than the SGM.

Bibliography

[1] T. Mikazuki and N. Matsui, "Statistical design techniques for high-speed circuit boards with correlated distributions," *IEEE Trans. Comp. Pack. & Man. Tech. Part A*, vol. 17, no. 1, pp. 159–165, Mar. 1994.

[2] A. H. Zaabab, Q.-J. Zhang, and M. Nakhla, "A neural network modeling approach to circuit optimization and statistical design," *IEEE Trans. Microw. Theory Tech.*, vol. 43, no. 6, pp. 1349–1358, Jun. 1995.

[3] Q. Zhang, J. J. Liou, J. McMacken, J. Thomson, and P. Layman, "Development of robust interconnect model based on design of experiments and multiobjective optimization," *IEEE Trans. Electron Devices*, vol. 48, no. 9, pp. 1885–1891, Sep. 2001.

[4] G. S. Fishman, *Monte Carlo: Concepts, Algorithms, and Applications*. New York: Springer-Verlag, 1996.

[5] H. Niederreiter, P. Hellekalek, G. Larcher, and P. Zinterhof, *Monte Carlo and Quasi-Monte Carlo Methods*. New York: Springer-Verlag, 1998.

[6] R. G. Ghanen and P. D. Spanos, *Stochastic Finite Elements. A Spectral Approach*. New York, USA: Springer-Verlag, 1991.

[7] D. Xiu, "Fast numerical methods for stochastic computations: A review," *Communications in Computational Physics*, vol. 5, no. 2-4, pp. 242–272, Feb. 2009.

[8] Q. Su and K. Strunz, "Stochastic circuit modelling with Hermite polynomial chaos," *Electronic Letters*, vol. 41, no. 21, pp. 1163–1165, Oct. 2005.

[9] S. Vrudhula and J. M. W. P. Ghanta, "Hermite polynomial based interconnect analysis in the presence of process variations," *IEEE Trans. Comput. Aided Design Int. Circ. Syst.*, vol. 25, no. 10, pp. 2001–2011, Oct. 2006.

[10] K. Strunz and Q. Su, "Stochastic formulation of SPICE-type electronic circuit simulation with polynomial chaos," *ACM Trans. on Modeling and Computer Simulation*, vol. 18, no. 4, pp. 15:1–15:23, Sep. 2008.

[11] P. Sumant, H. Wu, A. Cangellaris, and N. Aluru, "Reduced-order models of finite elements approximations of electromagnetic devices exhibiting statistical variability," *IEEE Trans. Antennas Propag.*, vol. 60, no. 1, pp. 301–309, Jan. 2012.

[12] D. Spina, F. Ferranti, T. Dhaene, L. Kockaert, G. Antonini, and D. Vande Ginste, "Variability analysis of multiport systems via polynomial-chaos expansion," *IEEE Trans. Microw. Theory Tech.*, vol. 60, no. 8, pp. 2329–2338, Aug. 2012.

[13] I. S. Stievano, P. Manfredi, and F. G. Canavero, "Stochastic analysis of multiconductor cables and interconnects," *IEEE Trans. Electromagn. Compat.*, vol. 53, no. 2, pp. 501–507, May 2011.

[14] I. S. Stievano, P. Manfredi, and F. Canavero, "Parameters variability effects on multiconductor interconnects via Hermite polynomial chaos," vol. 1, no. 8, pp. 1234–1239, Aug. 2011.

[15] D. Vande Ginste, D. De Zutter, D. Deschrijver, T. Dhaene, P. Manfredi, and F. Canavero, "Stochastic modeling based variability analysis of on-chip interconnects," *IEEE Transactions on Components, Packaging and Manufacturing Technology*, vol. 2, no. 7, pp. 1182–1192, Jul. 2012.

[16] A. Taflove, *The Finite-Difference Time Domain Method*. Norwood: Artech House, 1995.

[17] C. R. Paul, *Analysis of Multiconductor Transmission Lines*. John Wiley & Sons, 1994.

[18] D. Xiu and G. E. Karniadakis, "The Wiener-Askey polynomial chaos for stochastic differential equations," *SIAM J. Sci. Comput.*, vol. 24, no. 2, pp. 619–644, 2002.

[19] P. Manfredi, D. Vande Ginste, D. De Zutter, and F. G. Canavero, "Improved polynomial chaos discretization schemes to integrate interconnects into design environments," *IEEE Microwave and Wireless Components Letters*, vol. 23, no. 3, pp. 116–118, Mar. 2013.

[20] K. S. J. L. Volakis and B. C. Usner, *Frequency Domain Hybrid Finite Element Methods for Electromagnetics*, ser. Synthesis Lectures on Computational Eelectromagnetics. Morgan & Claypool Publishers, 2006.

[21] P. Manfredi, D. Vande Ginste, D. De Zutter, and F. G. Canavero, "On the passivity of polynomial chaos-based augmented models for stochastic circuits," *IEEE Trans. on Circuits and Systems*, vol. PP, pp. 1–10, Jul. 2013.

[22] P. J. Davis and P. Rabinowitz, *Methods of Numerical Integration*, 2nd ed. Dover Publications, 2007.

[23] N. Nakhla, A. E. Ruehli, M. S. Nakhla, R. Achar, and C. Chen, "Waveform relaxation techniques for simulation of coupled interconnects with frequency-dependent parameters," *IEEE Trans. on Advanced Packaging*, vol. 30, no. 2, pp. 257–269, May 2007.

[24] R. C. Jaeger and T. N. Blalock, *Microelectronic Circuit Design*, 2nd ed. McGraw-Hill, 2004.

[25] A. Papoulis, *Probability, Random Variables, and Stochastic Processes*, 3rd ed. McGraw-Hill, 1991.

[26] M. A. Abramowitz and I. A. Stegun, *Handbook of mathematical functions*. New York: Dover Publications, Inc., 1970.

[27] S. Grivet-Talocia, I. S. Stievano, and F. G. Canavero, "Hybridization of FDTD and device behavioral-modeling techniques," *IEEE Trans. Electromagn. Compat.*, vol. 45, no. 1, pp. 31–42, Feb. 2003.

[28] J. Bäck, F. Nobile, L. Tamellini, and R. Tempone, "Stochastic spectral Galerkin and collocation methods for PDEs with random coefficients: A numerical comparison," in *Spectral and High Order Methods for Partial Differential Equations*, ser. Lecture Notes in Computational Science and Engineering, J. S. Hesthaven and E. M. Ronquist, Eds. Springer Berlin Heidelberg, 2011, vol. 76, pp. 43–62.

CHAPTER 4

Variability Analysis of Interconnects Terminated by Polynomial Nonlinear Loads

Based on the publication:
"Variability Analysis of Interconnects Terminated by Polynomial Nonlinear Loads",
To be presented at: *Electrical Design of Advanced Packaging and Systems Symposium (EDAPS), 2013 IEEE*,
Nara, Japan, 12 – 15 December 2013

In this chapter, we construct a stochastic modeling method for the analysis of variability effects on interconnect structures terminated by polynomial nonlinear loads. The technique is similar to the one presented in Chapter 3 to solve the pertinent stochastic Telegrapher's equations in time domain by means of the so-called stochastic Galerkin method in conjunction with FDTD. However, here, we focus on polynomial nonlinear boundary conditions, allowing the inclusion of nonlinear capacitors at the terminals of the lines. The proposed technique is validated and illustrated with an example, demonstrating its accuracy and efficiency.

4.1 Introduction

In this chapter, we rely on the research carried out in Chapter 3, for the variability analysis of interconnects that are terminated by nonlinear loads. Here, however, we focus on terminations described by *polynomial* I-V characteristics and we show that they can be dealt with via an alternative, closed-form and exact formulation. The goal is to more efficiently and accurately solve the governing stochastic Telegrapher's equations for transmission lines terminated, e.g, by nonlinear polynomial capacitors.

This chapter is organized as follows. The formulation of the BCs is carried out in Section 4.2 where special attention is devoted to the description of polynomial nonlinear loads and to their FDTD implementation. In Section 4.3, the formalism is validated and illustrated by applying it to the variability analysis of a microstrip line, terminated by a nonlinear capacitor that is described by a polynomial model. Conclusions are presented in Section 4.4.

4.2 Formalism

4.2.1 Boundary Conditions

To describe how to include nonlinear polynomial loads within the SGM framework, we consider a case study, i.e., a single uniform transmission line terminated by a nonlinear capacitor. The proper stochastic Telegrapher's equations are treated in the same way as presented in Section 3.2, leading to the augmented set of equations (3.4) in the $(K+1)$ unknown expansion coefficients v_k and i_k, $k = 0, \ldots, K$. Again, an adequate set of $(K+1)$ boundary conditions (BCs) needs to be constructed. These new BCs now evolve from the generators and *polynomial* loads attached to the terminals of the original stochastic line (3.1).

Consider a deterministic nonlinear load at the far-end $z = \mathcal{L}$ of the line, as shown in Fig. 4.1, described by a capacitance that is a polynomial function of degree N of the voltage across it :

$$i(\mathcal{L},t,\beta) = C(v(\mathcal{L},t,\beta))\,\frac{\partial}{\partial t}\,v(\mathcal{L},t,\beta), \tag{4.1}$$

with

$$C(v(\mathcal{L},t,\beta)) = \sum_{n=0}^{N} C_n\,(v(\mathcal{L},t,\beta))^n, \tag{4.2}$$

Now, we apply the PC expansions (3.2) to (4.1):

$$\sum_{k=0}^{K} i_k(\mathcal{L},t)\phi_k(\beta) = \sum_{n=0}^{N} C_n \left(\sum_{k=0}^{K} v_k(\mathcal{L},t)\phi_k(\beta)\right)^n \times \sum_{j=0}^{K} \frac{\partial}{\partial t} v_j(\mathcal{L},t)\phi_j(\beta), \tag{4.3}$$

By using the multinomial coefficient theorem, (4.3) becomes:

$$\sum_{k=0}^{K} i_k(\mathcal{L},t)\phi_k(\beta) = \sum_{j=0}^{K}\sum_{n=0}^{N}\sum_{k_0+k_1+\ldots+k_K=n} C_n \times \binom{n}{k_0,k_1,\ldots,k_K}\prod_{0\le r\le K}\phi_r(\beta)^{k_r}\phi_j(\beta) \times \prod_{0\le r\le K}(v_r(\mathcal{L},t))^{k_r}\frac{\partial}{\partial t}v_j(\mathcal{L},t), \tag{4.4}$$

where k_0, k_1, etc are integers and with the multinomial coefficient :

$$\binom{n}{k_0,k_1,\ldots,k_K} = \frac{n!}{k_0!k_1!\ldots k_K!}. \tag{4.5}$$

Galerkin weighting of (4.4) yields the $K+1$ new BCs, $\forall m = 0,\ldots,K$:

$$i_m(\mathcal{L},t) = \sum_{j=0}^{K}\tilde{C}_{mj}(\mathcal{L},t,v_0,\ldots,v_K)\frac{\partial}{\partial t}v_j(\mathcal{L},t), \tag{4.6}$$

where

$$\tilde{C}_{mj}(\mathcal{L},t,v_0,\ldots,v_K) = \sum_{n=0}^{N}\sum_{k_0+\ldots+k_K=n} C_n\binom{n}{k_0,k_1,\ldots,k_K} \times < \prod_{0\le r\le K}(\phi_r(\beta))^{k_r}\phi_j(\beta),\phi_m(\beta) > \prod_{0\le r\le K}(v_r(\mathcal{L},t))^{k_r} \tag{4.7}$$

It is worth noticing that the factor $C_n\binom{n}{k_0,k_1,\ldots,k_K} \times < \prod_{0\le r\le K}(\phi_r(\beta))^{k_r}\phi_j(\beta),\phi_m(\beta) >$ is merely a real number. Therefore, despite the somewhat bulky equation (4.7), the new BCs are relatively simple and can be easily implemented in the SGM framework (see further). Also, in contrast to Chapter 3, the BCs are obtained in an analytical way, making them exact. The derivation of the BCs for, e.g, a polynomial conductance can be obtained in a similar way.

4.2.2 Implementation via the Finite-Difference Time-Domain (FDTD) Method

The solution to the augmented set of equations (3.4) in conjunction with the set of nonlinear BCs (4.7) is obtained by adopting the FDTD technique described in Chapter 3. After discretization of the Telegrapher's equations (3.4), the FDTD-leapfrog scheme (3.13), (3.14) is obtained, with special update functions (3.15), (3.16) at the

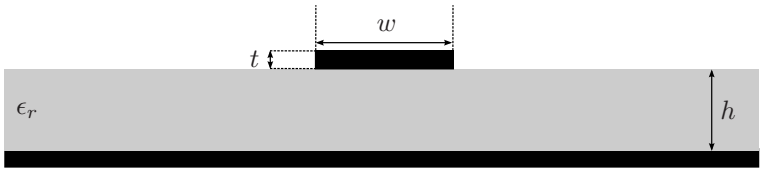

(a) Cross-section of the source-line-load configuration (Fig. 4.1(b)), where $w = 100$ μm, $h = 500$ μm and $t = 35$ μm. The width w of the line and the relative permittivity ϵ_r of the substrate are stochastic parameters.

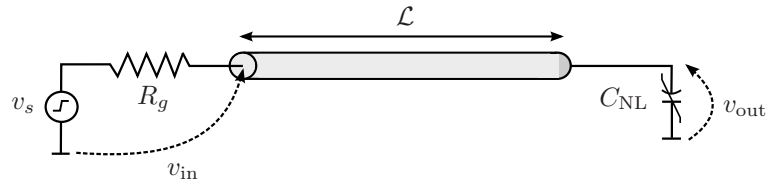

(b) Source-line-load configuration, where $\mathcal{L} = 5$ cm, $v_s(t)$ is a finite voltage step, $R_g = 50\ \Omega$, and with a nonlinear capacitor $C_{\rm NL}$.

Figure 4.1: Microstrip line under study.

terminals of the line. For a nonlinear capacitor, attached to the far-end of the line, the augmented BC in its discretized form, is given by

$$\tilde{i}_{fe,m}^{q+\frac{1}{2}} = \sum_{j=0}^{K} \tilde{C}_{mj} \frac{\tilde{v}_{N_z,m}^{q+1} - \tilde{v}_{N_z,m}^{q}}{2\Delta t} \tag{4.8}$$

where the coefficients $\tilde{C}_{mj}$ are given by (4.7). Next, the augmented BC are handled within our FDTD scheme implemented in Matlab, in particular making use again of the *fsolve.m* routine, which allows to find the roots of a nonlinear equation.

4.3 Numerical Results

In this section, the proposed approach is validated and illustrated by applying it to the variability analysis of a single PEC microstrip line. The results shown below have been obtained performing a set of simulations using an Intel(R) i7 (TM) QuadCore 2600K, with a clock speed of 3.4 GHz and 16 GB of RAM. The cross-section of the analyzed structure is presented in Fig. 4.1(a), while the source-line-load configuration is reported in Fig. 4.1(b), where $w = 100$ μm, $h = 500$ μm and $t = 35$ μm. The relative permittivity ϵ_r of the substrate and the line width w are considered to be two Gaussian RVs with mean $\mu_{\epsilon_r} = 4$ and $\mu_w = 100$ μm, respectively, and with normalized standard deviations $\sigma_{\epsilon_r} = 5\%$ and $\sigma_w = 5\%$. The microstrip line is excited by means of a voltage source $v_s(t)$ that produces a finite step, going from 0 V to 1 V in a

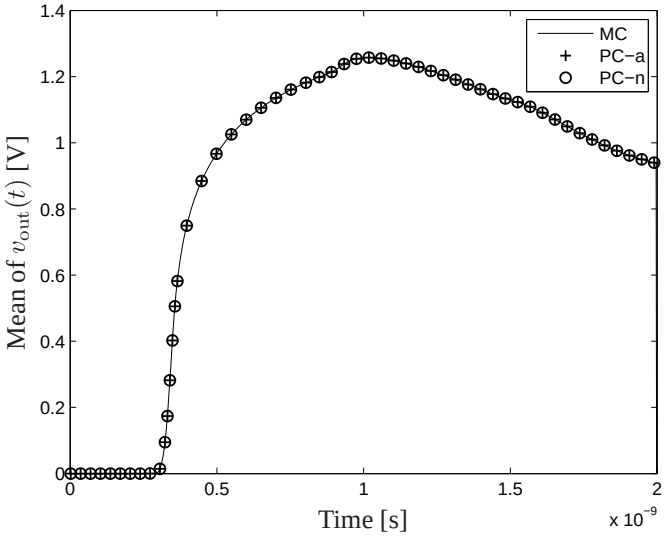

Figure 4.2: Mean of the voltage waveform $v_{\rm out}(t)$, at the terminal of the microstrip line of Fig. 4.1 obtained with MC and PC. Continuous line: MC technique; Crosses ($+$): newly proposed PC analytical technique (PC-a); Circles ($\circ$): numerical PC technique (PC-n), presented in Chapter 3. For clarity, results are only shown up to 2 ns.

risetime of 50 ps. The generator impedance is $R_{g1} = 50\,\Omega$. The nonlinear capacitance $C_{\rm NL}$ is characterized by (4.2) with $N = 2$ and with the following polynomial coefficients: $C_0 = 1\ pF$, $C_1 = -3\ pF/V$, $C_2 = 5\ pF/V^2$. Such a nonlinear capacitor could, e.g., represent a MOSFET's gate capacitance, but of course, any polynomial model can be handled with the proposed technique.

In order to obtain a reference result, a set of 10000 MC simulations was performed. The obtained results are also compared to the ones computed using the purely numerical approach proposed in Chapter 3, i.e. without exploiting the polynomial behavior of the nonlinear capacitor. In Fig. 4.2 the mean of the voltage at the output obtained using the two PC-based methods (analytical and numerical) is compared with the result of the reference MC method. For clarity of the figure, results are only shown up to 2 ns. Next, the comparison between the standard deviation computed by means of the proposed method, the MC reference and the numerical solution in Chapter 3 is reported in Fig. 4.3. We observe an excellent agreement between all the results. Moreover, the total runtime for the MC analysis was 41880 s, whereas the novel SGM simulation only took 45 s. By using the SGM technique presented in Chapter 3, the total runtime was 79 s. Hence, the proposed technique provides a speedup of ca. $930\times$ compared to the reference MC method, and, by analytically exploiting the polynomial characteristic of the load, it also outperforms the more general, but purely numeri-

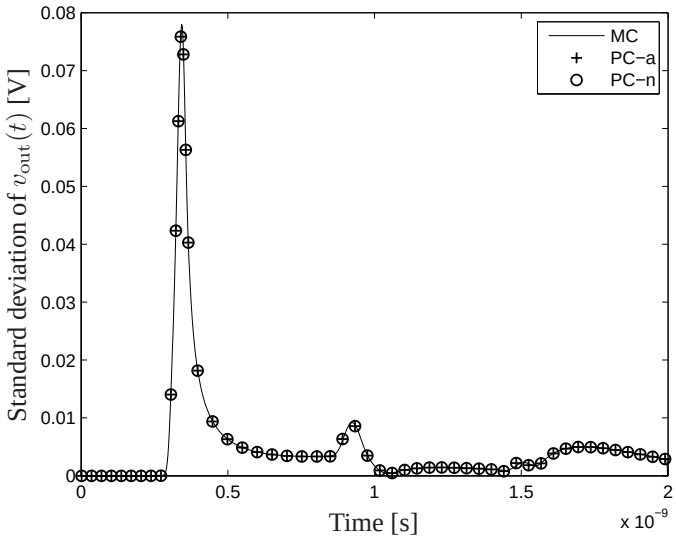

Figure 4.3: Standard deviation of $v_{\rm out}(t)$, obtained with MC and PC. Continuous line: MC technique; Crosses ($+$): newly proposed PC analytical technique (PC-a); Circles ($\circ$): numerical PC technique (PC-n), presented in Chapter 3. For clarity, results are only shown up to 2 ns.

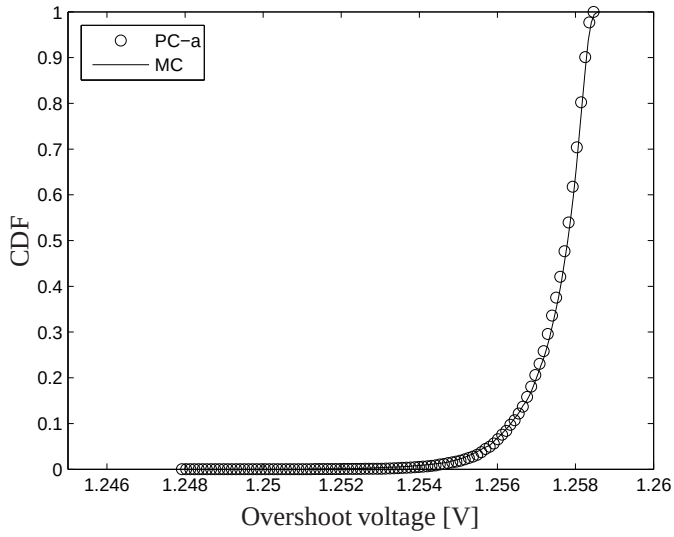

Figure 4.4: Cumulative distribution function of $max(v_{\rm out}(t))$

cal, technique presented in Chapter 3. Further, we present the cumulative distribution function (CDF) of the maximum of the output voltage, reported in Fig. 4.4. Apart from the excellent agreement between MC and the new technique, from this figure, the maximum overshoot that one can expect, is readily assessed.

4.4 Conclusions

In this chapter we have adapted the PC-based technique of Chapter 3 for stochastic circuits in order to more effectively deal with nonlinear terminations described by a polynomial I-V characteristic. The technique is based on combining the SGM with FDTD. It was validated and illustrated by means of an application example, consisting of a microstrip line exhibiting variability of its geometrical and material parameters, and terminated with a nonlinear polynomial capacitance. The results have been compared to a standard and robust Monte Carlo analysis, and to the numerical method presented in Chapter 3. This comparison shows an excellent agreement, and as expected, an improved efficiency in comparison to both MC and the numerical method.

CHAPTER 5

Variability Analysis of Interconnect Structures Including General Nonlinear Elements in a SPICE-type Framework

Based on the publication:

"Variability Analysis of Interconnect Structures Including General Nonlinear Elements in a SPICE-type Framework",
submitted for publication in *IET Electronic Letters*.

In this chapter, the stochastic method developed in Chapter 3 is adapted to be implemented in a SPICE framework to analyze variability effects on interconnect structures including general nonlinear elements.

5.1 Introduction

So far, PC-based techniques relying on the SGM were mainly developed in Matlab. This technique has also been employed for distributed circuits including only linear elements and for these types of problems the method was modified in [1] to allow implementation in a SPICE environment. As far as *nonlinear* elements are concerned, a PC-method for lumped circuits consisting of discrete, linear and nonlinear elements was first reported in [2, 3], allowing to model uncertainties in a small-signal regime

or by approximating the nonlinearities by means of Taylor expansions. In Chapter 3 we reported a stochastic method developed for the variability effects on interconnect structures including *general* nonlinear elements. Unfortunately, this technique could solely be implemented in Matlab, as it relies on a FDTD solver for transmission lines, making it also cumbersome to deal with lossy, dispersive lines and arbitrary circuit topologies. Therefore, in the present chapter, a SPICE-compatible method is developed and implemented in a traditional environment allowing for the first time to perform PC-based variability analyses of lossy, dispersive multiconductor transmission lines terminated by general nonlinear loads. The goal is to make this technique more accessible for designers when implemented in a commercial tool.

This chapter is organized as follows. The formulation of the BCs is carried out in Section 5.2 where special attention is devoted to the description of general nonlinear loads and to their SPICE implementation. In Section 5.3, the formalism is validated and illustrated by applying it to the variability analysis of a multiconductor microstrip line, terminated by a diode, described by a nonlinear I-V-characteristic, and by a linear capacitor. Conclusions are presented in Section 5.4.

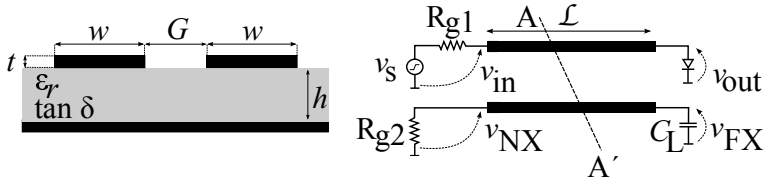

Figure 5.1: Cross-section AA' (left) of the source-line-load configuration (right) of a pair of coupled microstrip lines.

5.2 Stochastic Modeling Formalism and Implementation

In this section we discuss the formalism used to obtain a proper set of BCs to be implemented in a SPICE framework. The proper stochastic Telegrapher's equations are treated in the same way as presented in Section 3.2, leading to the augmented set of equations (3.4) in the $2(K+1)$ unknown expansion coefficients v_k and i_k, $k = 0, \ldots, K$.

To solve the set of $2(K+1)$ equations in (3.4), a set of $2(K+1)$ BCs is required. These are obtained by adding terminations to the lines. Assume that a nonlinear load is attached to the far-end terminal, i.e. at $z = \mathcal{L}$, with the following characteristic:

$$i(\mathcal{L}, t, \beta) = F(v(\mathcal{L}, t, \beta)), \tag{5.1}$$

where $F(\cdot)$ represents a general nonlinear function. Then, it was shown in Chapter 3 that by means of the SGM a new set of $K+1$ deterministic BCs is obtained, which can be cast in the form:

$$\forall m = 0, \ldots, K: \quad \tilde{i}_m(\mathcal{L}, t) \approx \sum_{q=1}^{Q} w_{mq}^{(1)} \, F\left(\sum_{k=0}^{K} w_{kq}^{(2)} \tilde{v}_k(\mathcal{L}, t) \right), \tag{5.2}$$

where $w_{mq}^{(1)}$ and $w_{kq}^{(2)}$ are weights ($k, m = 0, \ldots, K$; $q = 1, \ldots, Q$) and Q is a parameter that determines the accuracy. A similar set of BCs can be obtained at the near end $z = 0$, for any kind of (non)linear load and generator. The novel BCs (5.2) connect all voltage and current expansion coefficients contained in $\tilde{\mathbf{v}}$ and $\tilde{\mathbf{i}}$ through the known nonlinear function $F(\cdot)$ and proper linear combinations. Hence, these deterministic BCs (5.2) are readily implemented in a SPICE framework, using dependent sources. This results in a somewhat more complex network in terms of number of nodes, but guarantees a very efficient simulation yielding comprehensive statistical information, and rendering this technique very useful for variability analysis during circuit design.

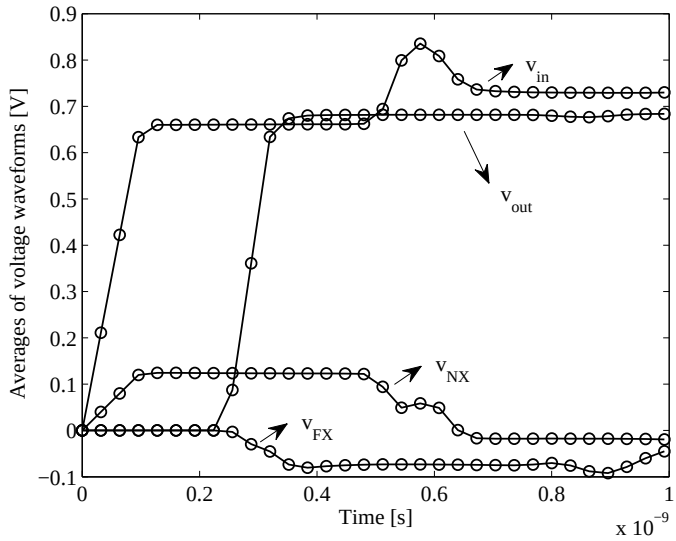

Figure 5.2: Averages of the voltage waveforms $v_{\rm in}(t)$, $v_{\rm out}(t)$, $v_{\rm NX}(t)$, and $v_{\rm FX}(t)$, at the four terminals of the coupled microstrip lines of Fig.5.1. Circles ($\circ$): average computed using the SGM technique; full black lines: average computed using the MC technique.

5.3 Numerical Results

In this section the technique is validated by applying it to the variability analysis of the pair of coupled copper microstrip lines illustrated in Fig. 5.1. The length $\mathcal{L}$ is $5\ cm$ and the gap G between the lines and the relative permittivity ϵ_r of the substrate are considered to be two RVs uniformly distributed in the range $[70, 90]$ μm and $[3.7, 4.3]$, respectively. The first line, i.e. the active line, is excited by means of a voltage source $v_s(t)$ that produces a ramped step, going from 0 V to 1 V in a risetime of 100 ps, in series with an impedance $R_{g1} = 50\ \Omega$. This active line is terminated by means of a forward biased diode described by the well-known Shockley-model $i = I_s \left(e^{\frac{v}{\eta V_t}} - 1 \right)$, where $I_s = 5 \cdot 10^{-14}$ A, $\eta = 1$, and $V_t = 25.85$ mV. The second line, called the victim line, is terminated at the near-end by a $50\ \Omega$ load R_{g2}. At the far-end, a 1 pF ideal capacitor C_L is connected. We chose to monitor the voltage waveforms $v_{\rm in}$ at the input of the active line, $v_{\rm out}$ at the diode, the near-end crosstalk $v_{\rm NX}$ and the far-end crosstalk $v_{\rm FX}$, all indicated on Fig. 5.1. The results

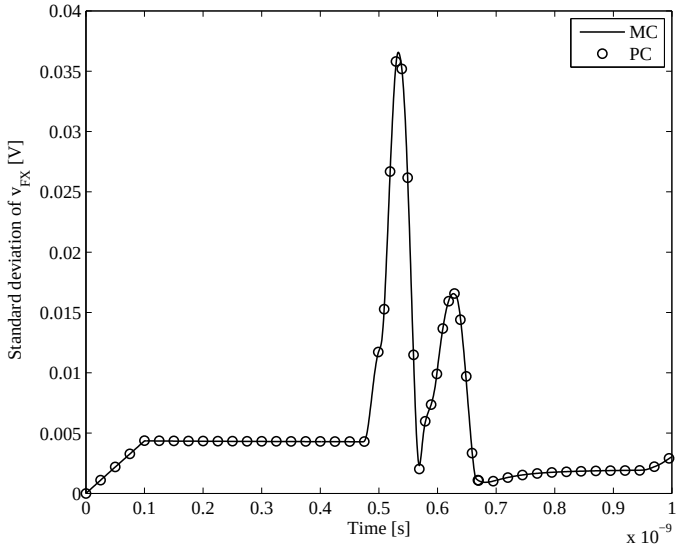

Figure 5.3: Standard deviation of the far-end crosstalk $v_{\rm FX}(t)$. Circles (○): SGM technique; black line: MC technique.

are shown in Fig. 5.2, where the continuous black lines represent the averages of the voltage waveforms obtained by performing a MC simulation in HSPICE, using 10000 samples of G and ϵ_r, drawn according to their respective uniform distributions. The proposed SGM approach for nonlinear loads was implemented and simulated also in HSPICE. The parameter K was set to 5 and all losses, i.e. copper conductivity

$\sigma = 5.8 \times 10^7 S/m$ and substrate losses $\tan\delta = 0.02$, were taken into account. The results of the proposed SGM are plotted as circles in Fig. 5.2. In Fig. 5.3 the standard deviation of $v_{\rm FX}(t)$ is presented. For both stochastic moments, i.e. average and standard deviation shown in Figs. 5.2 and 5.3, respectively, a very good agreement compared to the reference result is obtained.

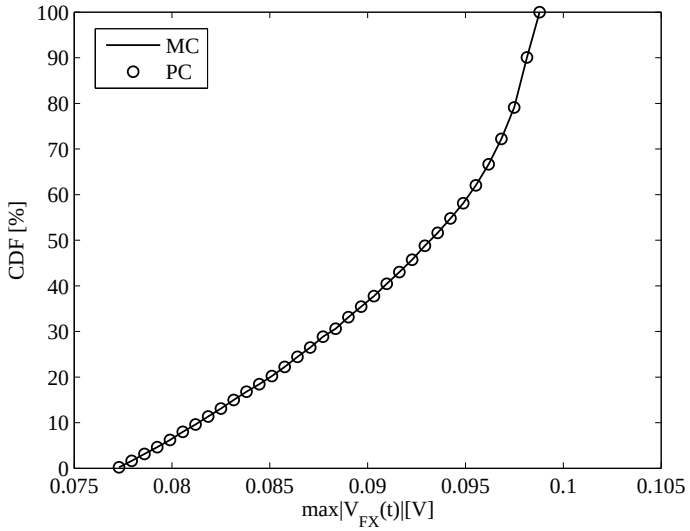

Figure 5.4: CDF of the maximum of the far-end crosstalk for $v_{\rm FX}(t)$.

All computations have been performed using HSPICE on a Dell Latitude E6500 laptop with an Intel(R) Core(TM) 2 Duo T9900 CPU running at 3.06 GHz and 4 GB of RAM. The total runtime for the MC analysis was 5656.4 s, the SGM simulation only took 1.11 s. A remarkable speed-up factor exceeding 5000 is obtained by means of the SGM approach.

Usually, designers are interested in quantifying the maximum amount of crosstalk that can be expected from a certain topology. Therefore, in a post-processing step and in addition to stochastic moments, we compute the CDF of the maximum far-end crosstalk, $\max_{t\geq 0}|v_{\rm FX}(t)|$. From Fig. 5.4, an excellent agreement between the MC simulations and the novel approach is again observed.

5.4 Conclusion

A stochastic method was developed and implemented in a SPICE-type framework for the variability analyses of lossy, dispersive MTLs in the presence of *general* nonlinear loads. The methodology was validated and illustrated in the HSPICE environment

by means of an example consisting of a pair of coupled microstrip lines exhibiting variability of its geometrical and material parameters, terminated by a nonlinear diode. Compared to the standard MC analysis, this method delivers an excellent agreement and shows superior efficiency.

Bibliography

[1] P. Manfredi, D. Vande Ginste, D. De Zutter and F. G. Canavero, “Uncertainty assessment of lossy and dispersive lines in SPICE-type environments”, *IEEE Trans. on Components, Packaging and Manufacturing Technology*, vol. 3, pp. 1252-1258, Jul. 2013.

[2] Q. Su and K. Strunz, “Stochastic circuit modelling with Hermite polynomial chaos”, *Electronic Letters*, vol. 41, pp. 1163-1165, Oct. 2005.

[3] K. Strunz and Q. Su, “Stochastic formulation of SPICE-type electronic circuit simulation with polynomial chaos”, *ACM Trans. on Modeling and Computer Simulation*, vol. 18, pp.15:1-15:23, Sep. 2008.

CHAPTER 6
Conclusions and Future Research

The research presented in this doctoral thesis focused on EM-aware characterization and modeling of nonlinear circuits. This final chapter summarizes the obtained results and outlines some potential directions for future research.

6.1 Conclusions

Standard EMC testing procedures most often focus on single-source/single-frequency illumination of the devices under test. There are no conventional test practices that involve multi-source/multi-frequency testing. Therefore, we have proposed a new experimental technique to characterize intermodulation distortion phenomena that typically occur in noisy EM environments, which contain multiple (co-located) sources. This new approach is suitable for any generic DUT composed of at least one active non-linear component and a passive susceptible antenna by clearly defining a set of pertinent measurement scenarios. By means of a vector network analyzer that allows nonlinear analysis, such as Agilent's PNA-X, and in a controllable environment, preferably an anechoic chamber, we showed that intermodulation products, desensitization, etc., induced by a combination of desired, in-the-band, and undesired, out-of-band, signals can be accurately quantified.

Next to characterization, we have also shown that the modeling of nonlinear circuits, subjected to high-frequency phenomena, requires special attention. In particular, this is the case for high-speed interconnect structures, as their manufacturing process causes geometrical and material parameter uncertainties. This variability leads to nondeterministic behavior, and hence necessitates the development of stochastic modeling tools. In recent literature, polynomial chaos (PC) based techniques have been developed for lumped circuits and distributed interconnects, proving their ability for accurate and efficient variability analysis. However, so far, stochastic inter-

connect structures could only be terminated by linear loads and PC-based techniques for stochastic lumped circuits could only take mild nonlinearities into account. The novel SGM-FDTD framework, advocated in Chapter 3, is capable of also including general nonlinear loads, described by arbitrary I-V-characteristics, at the terminals of stochastic multiconductor transmission line. This opens up a much wider range of applications that can now be tackled. The technique was validated and illustrated by means of an application example, consisting of a pair of coupled microstrip lines exhibiting variability of its geometrical and material parameters, and terminated by a diode with a non-smooth I-V-characteristic. Compared to a standard, robust Monte Carlo analysis, the method showed excellent agreement and far superior efficiency.

In Chapter 4, the SGM-FDTD technique is refined to deal with a special class of nonlinear components that exhibit a polynomial I-V-characteristic. This polynomial behavior is exploited by calculating the pertinent integrals, occurring in the SGM-FDTD scheme, analytically rather than via Gaussian quadrature rules, making the technique less computationally demanding after implementation. This was validated and illustrated by means of an application example, consisting of a microstrip line exhibiting variability of its geometrical and material parameters, and terminated with a nonlinear polynomial capacitance. The results have been compared to a standard and robust Monte Carlo analysis, and to the numerical method presented in Chapter 3. This comparison shows an excellent agreement, and as expected, an improved efficiency in comparison to both Monte Carlo and the numerical method.

The SGM-FDTD techniques of Chapters 3and 4 were implemented in Matlab. To make the techniques more accessible for design engineers, in Chapter 5 the stochastic method was adapted for implementation in a SPICE-type framework. Here, again, the goal is to analyze the variability of MTLs in the presence of general nonlinear loads, and thanks to the novel implementation, lossy and dispersive lines can now be treated as well. The methodology was validated and illustrated in the HSPICE environment by means of an example consisting of a pair of coupled microstrip lines exhibiting variability of its geometrical and material parameters, terminated by a nonlinear diode. Compared to the standard Monte Carlo analysis, this method delivers an excellent agreement and shows superior efficiency.

6.2 Future Research

This dissertation highlighted the importance of devising new characterization and modeling techniques for nonlinear circuits, subjected to adverse phenomena, such as unwanted noise or parameter variability. Clearly, techniques as presented in this work are becoming indispensable for state-of-the-art design and therefore, further developments are imperative.

Future research dedicated to the EM-aware characterization of active nonlinear components has to consider the presence of a higher number of transmitting (co-

located) sources, as such mimicking a more realistic environment. Also, new strategies to evaluate more complex architectures such as commercial devices that comprise multi-band antennas directly connected to active components should be developed. From an EMC standardization viewpoint, compliance tests should contemplate the immunity of devices under tests w.r.t. radiated emissions by multiple sources. Therefore, an international agreement is needed on, e.g., more advanced testing scenarios, eventually leading to standardization. Also, it is relevant to investigate how the immunity defined by the aforementioned tests gets influenced in the presence of manufacturing tolerances (permittivity of the substrate, deviation of the geometrical parameters due to the etching, etc.). Combining statistical analysis with the EM-aware characterization would lead to a completely new class of experimental methodologies, improving the overall EMC and SI performance of novel devices.

Considering the statistical analysis framework, future research should focus on the inclusion of (behavioral models of) *dynamic* nonlinear terminations, as well as on the extension of the application examples to I/O bus structures with many random variables. With respect to the latter extension, the scalability of the SGM becomes an issue that requires further study. Additionally, a comparison with non-intrusive stochastic modeling techniques, such as the stochastic collocation method (SCM), would be useful, as the SCM is probably more parallelizable than the SGM.

In summary, it can be stated that it is of critical importance to invest in new characterization and modeling techniques for nonlinear circuits, as this will in the end allow to efficiently conceive new devices, avoiding time-consuming and costly redesigns. In the presented work, it was shown that combining standard circuit models with stochastic simulation methods leads to reliable variability analysis, which can be easily adopted by hardware designers. Also, leveraging more complex and realistic experimental techniques are important for the development of new electronic devices. The author believes that more research in this crucial domain will and has to be performed over the coming years.